

Lawrence Berkeley National Laboratory

LBL Publications

Title

Quantifying carbon budget, crop yields and their responses to environmental variability using the ecosys model for U.S. Midwestern agroecosystems

Permalink

<https://escholarship.org/uc/item/4b50k99f>

Authors

Zhou, Wang

Guan, Kaiyu

Peng, Bin

et al.

Publication Date

2021-09-01

DOI

10.1016/j.agrformet.2021.108521

Peer reviewed

1 **Quantifying carbon budget, crop yields and their responses to**
2 **environmental variability using the *ecosys* model for U.S.**
3 **Midwestern agroecosystems**

4
5
6 **Wang Zhou^{1,2,*}, Kaiyu Guan^{1,2,3,*}, Bin Peng^{1,2,3,*}, Jinyun Tang⁴, Zhenong Jin⁵, Chongya**
7 **Jiang^{1,2}, Robert Grant⁶, and Symon Mezbahuddin^{6,7}**

8 ¹Agroecosystem Sustainability Center, Institute for Sustainability, Energy, and Environment,
9 University of Illinois at Urbana Champaign, Urbana, IL 61801, USA

10 ²College of Agricultural, Consumer and Environmental Sciences, University of Illinois at Urbana-
11 Champaign, Urbana, IL, USA

12 ³National Center for Supercomputing Applications, University of Illinois at Urbana-Champaign,
13 Urbana, IL, USA

14 ⁴Earth and Environmental Sciences Area, Lawrence Berkeley National Laboratory, Berkeley, CA,
15 USA

16 ⁵Department of Bioproducts and Biosystems Engineering, University of Minnesota, St. Paul, MN,
17 USA

18 ⁶Department of Renewable Resources, University of Alberta, Edmonton, AB, Canada

19 ⁷Natural Resource Management Branch, Alberta Agriculture and Forestry, Edmonton, AB, Canada

20 Corresponding to: Kaiyu Guan (kaiyug@illinois.edu); Bin Peng (binpeng@illinois.edu); Wang Zhou
21 (wangzhou@illinois.edu)

22

23

24 **Abstract:**

25 As one of the major agricultural production areas in the world, the United States (U.S.)
26 Midwest plays a vital role in the global food supply and agricultural ecosystem services. Although
27 significant efforts have been made in modeling the carbon cycle dynamics over this area, large
28 uncertainty still exists in the previous simulations in terms of reproducing individual components
29 of the carbon cycle and their responses to environmental variability. Here we evaluated the
30 performance of an advanced agroecosystem model, *ecosys*, in simulating carbon budgets over the
31 U.S. Midwest, considering both the magnitude of carbon flux/yield and its response to the
32 environmental (climatic and soil) variability. We conducted model simulations and evaluations at
33 7 cropland eddy-covariance sites as well as over 293 counties of Illinois, Indiana, and Iowa in the
34 U.S. Midwest. The site-level simulations showed that *ecosys* captured both the magnitude and
35 seasonal patterns of carbon fluxes (i.e., net ecosystem carbon exchange, ecosystem gross primary
36 production (GPP), and ecosystem respiration), leaf area index, and dynamic plant carbon allocation
37 processes, with R^2 equal to 0.92, 0.87, 0.87, and 0.78 for GPP, NEE, Reco, and LAI, respectively
38 across all the sites compared with the observations. For regional scale simulations, *ecosys*
39 reproduced the spatial distribution and interannual variability of corn and soybean yields with the
40 constraints of observed yields and a new remotely sensed GPP product, with R^2 of multi-year
41 averaged simulated and observed yield equal 0.83 and 0.80 for corn and soybean, respectively.
42 The simulated responses of carbon cycle dynamics to environmental variability were consistent
43 with that from the empirical observations at both site and regional scales. Our results demonstrated
44 the applicability of *ecosys* in simulating the carbon cycle and soil carbon sequestration of the U.S.
45 Midwestern agroecosystems under different climate and soil conditions.

46 **Keywords:** carbon fluxes, crop yield, *ecosys*, agroecosystems, environmental variabilities, U.S.
47 Midwest

48

49 **1. Introduction**

50 The terrestrial carbon balance of agroecosystems plays an important role in the global
51 carbon cycle (Dold et al., 2017; Verma et al., 2005). Depending on the temporal and spatial scales
52 used for accounting as well as the geographical regions, croplands can be either carbon sinks or
53 sources for the atmospheric CO₂ (Blanco-Canqui and Lal, 2004; Kimble et al., 1998). In the U.S.
54 Midwest, about 30–50% of soil organic carbon (SOC) has been lost when compared with that
55 before cultivation for most croplands (Lal, 2002). Since SOC content is often positively related to
56 soil fertility, SOC loss may enhance crop yield loss risk under future climate conditions (Lal, 2011,
57 2004, 2001). Fortunately, with recommended management practices (RMPs, i.e., conservation
58 tillage, cover crops, and biosolids and manure, etc.), prior studies show that U.S. croplands have
59 the potential to sequester about 75–208 Tg C/year, which may recover 50–70% of the depleted soil
60 carbon (Jarecki and Lal, 2003; Lal, 2011, 2007, 2002; Meena et al., 2020; Hutchinson et al., 2007;
61 Chambers et al., 2016). Hence, in order to help realize this carbon sequestration potential in U.S.
62 croplands, and meanwhile ensure global food security, it is critical to accurately quantify the
63 carbon balance of agroecosystems, including carbon fixation and emission.

64 The carbon inventory (West et al., 2013, 2010, 2008; West and Marland, 2002), derived
65 from crop yield survey reports (Vogel, 2018), SOC measurements (van Wesemael et al., 2010),
66 and observation-based gross primary production (GPP) estimations (Jiang et al., 2021), can
67 provide several components of cropland carbon budget. Among these carbon inventory methods,
68 soil-sampling-based SOC measurement is the most direct approach to investigate SOC change, but

69 it still has uncertainties associated with soil sampling strategies (i.e., sampling location, depth, and
70 time), measurement methods, and duration of measurements (Jandl et al., 2014; Schrumpf et al.,
71 2011; VandenBygaart and Angers, 2006). More importantly, it is difficult to scale up the soil
72 sampling due to its high labor and financial costs. In the framework of carbon balance, SOC change
73 can in principle be derived from the whole carbon mass balance, which requires different carbon
74 cycling components (i.e., GPP, ecosystem respiration, and harvest etc.). However, most of the
75 carbon inventories cover only part of the carbon cycling components, such as agroecosystem
76 carbon input (i.e., GPP) or outputs (i.e., yield). Measurements of other key carbon cycling
77 components (i.e., respiration and litterfall) of agroecosystems are still difficult and insufficient,
78 especially at large scales (e.g. U.S. Midwest) (Osborne et al., 2010). All these factors limit wide
79 and robust applications of carbon inventory to quantify agroecosystem carbon budgets and SOC
80 change.

81 Alternatively, we can use process-based models to quantify the cropland carbon budget
82 (Brilli et al., 2017; Huang et al., 2009; Wattenbach et al., 2010; Zhang et al., 2015). However,
83 existing studies using process-based models for cropland carbon quantification have suffered from
84 one or few of the following limitations. First, very few model-based quantifications of the cropland
85 carbon budget have gone through rigorous model validation covering the whole agroecosystem
86 carbon cycle (i.e., carbon fixation, carbon allocation, and respiration), especially at regional scales.
87 Most process-based modeling studies for agroecosystems evaluated and constrained their models
88 with a limited number of observational variables, such as crop yield (Gilhespy et al., 2014; Stehfest
89 et al., 2007) and/or measured SOC (Li et al., 1997; Liu et al., 2006; Shirato, 2005). This lack of
90 sufficient model constraint may cause simulations to be apparently right with wrong reasons (Peng
91 et al., 2018). For example, models can generate the same crop yield with higher carbon fixation

92 but lower harvest index compared to the correct ones, because errors in plant carbon fixation can
93 be reconciled by unconstrained fluxes of respiration and litterfall. Therefore, to ensure that the
94 model simulates carbon emission and sequestration correctly in both short and long terms, we need
95 to use more carbon-related observations with fine temporal resolution (i.e., daily GPP, NEE, Reco,
96 LAI, plant carbon allocation, and phenology) to sufficiently constrain and validate the carbon
97 cycling processes of the models.

98 Second, most existing model-based studies only calibrated and validated the models at a
99 few specific sites due to limited availability of observations. In general, models involve both
100 parameters that are site-specific (i.e., maturity group and climate zone) and parameters that are
101 shared among sites at a regional scale (i.e., parameters controlling the temperature responses of
102 activity of RuBP carboxylase-oxygenase) (Kuppel et al., 2012; Mäkelä et al., 2007). Thus
103 optimizing a model at specific sites will tie the resultant model parameterization closely to the site
104 information (e.g. climate, soil, groundwater depth, field microtopography, and land management
105 practices etc.), so that the model may not be suitable for other sites and regions with different soil
106 and climate conditions. To ensure the model parameterization can be robustly transferred to other
107 sites or regions, systematic evaluations are needed. Specifically, we need to constrain and evaluate
108 models under a wide range of soil and climate conditions, using diverse data such as large-scale
109 carbon inventories (e.g. crop yield reports and crop progress reports) and satellite remote sensing
110 carbon-related observations (e.g. GPP and LAI).

111 Finally, current model calibrations and validations have generally focused on matching the
112 magnitude or time series of the target variables (e.g., GPP and yield) (Gurung et. al., 2020; Wang
113 et al., 2020; Jin et al., 2017), which is achieved by minimizing a cost function (which measures
114 model-data discrepancy) that does not take into account the relationship between these target

115 variables and environmental drivers. From the perspective of Bayesian inference (Tarantola, 2013),
116 since only uncertainties in model parameters are constrained, such a practice leads to an
117 underestimation of the prior information associated with the environmental drivers. To make a
118 more comprehensive use of the information contained in observations and model driving variables,
119 as well as to deliver more confident predictions of how agroecosystems will respond to
120 environment changes, we thus further need to verify relationships between environment variables
121 and model predicted variables to test whether the model can simulate emergent responses of those
122 variables to environmental factors from empirical observations (Peng et al., 2020). The accurate
123 representation of the response of the target variables to environmental factors (i.e., climate
124 variability and soil conditions) will help expand the models to broader soil and climate conditions.

125 Based on the above rationale, to demonstrate a new standard to achieve a comprehensive
126 constraint and evaluation of an agroecosystem simulator, in this study we used an advanced
127 ecosystem model, *ecosys*, to simulate surface carbon fluxes and corn/soybean yield in the U.S.
128 Midwest at both eddy-covariance sites and county scales for the three I states (Illinois, Iowa and
129 Indiana). As one of the world's largest crop production areas, the U.S. Midwest produces about
130 85% of U.S. corn and soybean (USDA, 2020). The soil health and crop yield of the U.S. Midwest
131 in the future is vital to the global food supply and agricultural ecosystem services. To improve the
132 quantification of carbon cycle dynamics in the U.S. Midwest, both the absolute values of the
133 simulated carbon fluxes and yield as well as the responses of those variables to the environmental
134 variabilities were evaluated. Through the evaluations, we aim to evaluate the capability of *ecosys*
135 in conducting spatiotemporal extrapolations of agroecosystem carbon cycle by addressing the
136 following two questions: (1) To what extent can *ecosys* simulate agroecosystem carbon dynamics
137 at different individual sites as well as across the broader regions in the U.S. Midwest? (2) How

138 well can *ecosys* capture responses of carbon fluxes and crop yield to environmental variabilities?
139 Although we use *ecosys* as an example, the procedures for model evaluation described in this study
140 are applicable to many other agroecosystem models.

141

142 **2. Data and method**

143 **2.1 The process-based model *ecosys***

144 *Ecosys* is an advanced mechanistic ecosystem model developed to simulate water, energy,
145 carbon, and nutrient cycles simultaneously for various ecosystems, including agroecosystems at
146 the hourly step (Figure 1a) (Grant, 2001). It is one of the very few models that are formulated
147 primarily based on biophysical and biochemical principles, with fully connected balances and
148 interactions for water, energy, carbon and nutrient cycles in the soil-plant-atmosphere continuum,
149 and has been extensively validated in various ecosystems ranging from agricultural (Grant et al.,
150 2007, 2011; Mezbahuddin et al., 2020) to forest systems (Grant et al., 2010, 2006).

151 The *ecosys* model was built based on the strategy that pursues the mechanistic
152 representations and model outputs as directly comparable to observations as possible to
153 realistically inform agricultural practices, by combining reactive transport modeling and state of
154 the art knowledge of biogeochemistry (Grant, 2001). For example, photosynthesis and plant
155 hydraulics in *ecosys* are coupled through leaf osmotic pressure, and then turgor pressure and leaf
156 water potential that is linked to stomatal conductance (Grant, 1995; Grant and Flanagan, 2007),
157 rather than empirical stress functions (Van den Hoof et al., 2011; Liu et al., 2016; Yokohata et al.,
158 2020), and all of which can be measured in the field (Salmon et al., 2020; Shekoofa et al., 2021;
159 Xue et al., 2021). As it integrates the plant hydraulics closely with the plant photosynthesis (Grant
160 et al., 1999), the plant stomata conductance in *ecosys* is directly controlled by the balance between

161 photosynthetic carbon assimilation and plant water hydraulics calculated for the soil-plant-
162 atmosphere continuum, which can properly resolve the plant response to drought (Mekonnen et
163 al., 2017). Due to the explicit simulation of plant hydraulic impacts on stomatal conductance, the
164 empirical crop response to atmospheric vapor pressure deficit does not need be prescribed as in
165 many other models (Van den Hoof et al., 2011; Liu et al., 2016; Yokohata et al., 2020). In response
166 to soil water and plant carbon stress, *ecosys* also dynamically adjusts the plants' carbon and
167 nutrient allocation strategies (Grant et al., 2001a), so that all plant organs will balance their
168 respective growth to help the plants survive the harsh growth conditions and flourish under
169 favorable conditions. In addition, the plant carbon and nutrient allocation is represented following
170 the source-storage-sink balance approach, rather than the fixed allometric relationship approach
171 adopted by most existing models (Grant, 1989b; Drewniak et al., 2013; Liu et al., 2016).

172 Moreover, *ecosys* employs much more complete physical and chemistry theories in
173 simulating soil related processes. Specifically, *ecosys* mechanistically resolves the oxygen stress
174 throughout the soil and plant roots (Grant, 1998), such that a flood condition will suppress plants'
175 growth and alter the soil carbon and nutrient cycling. In addition, *ecosys* explicitly includes
176 microbes' competitive and symbiotic nutrient interactions with plants (Grant and Pattey, 2003;
177 Grant et al., 2006; Grant and Pattey, 2008; Grant et al., 2016), enabling a nutrient-based analysis
178 of how various management practices could affect plant productivity. Meanwhile, soil organic
179 carbon dynamics in *ecosys* are driven explicitly by microbial community dynamics that emerge
180 from the interactions between bacteria and fungi, and another five functional groups carrying out
181 fermentation, methane and nitrogen cycling (Grant, 2013; Grant and Rochette, 1994). Emergent
182 microbial population structure, e.g. bacteria to fungi ratio, can be directly evaluated with respect
183 to field measurements (Anderson and Domsch, 1975; Bardgett and McAlister, 1999). Moreover,

184 the partitioning of soil carbon in *ecosys* is amenable to the density fractionation that is often used
 185 by empiricists to characterize soil organic matter. In addition, *ecosys* outputs profiles and fluxes
 186 of many easily measurable chemicals, including different phase existences of CO₂, CH₄, N₂O, NH₃,
 187 NO₃, HPO₄⁽²⁻⁾, etc. Finally, *ecosys* resolves many common agricultural practices, such as mixed
 188 cropping, depth dependent irrigation and tillage (Grant, 1997), banded vs broadcast fertilization
 189 (Grant et al., 2001b), soil liming, manure application (Grant et al., 2001c), denitrification inhibitor
 190 (Grant et al., 2020), and tile-drainage system (Mezbahuddin et al., 2017) etc. Finally, *ecosys*
 191 generally requires no calibration for the soil and hydrological processes due to its complete
 192 mechanistics thus provides scalability to regional scale applications (Grant et al., 2012). All these
 193 features make *ecosys* stand out as a unique simulator as compared to many other models that tend
 194 to lump processes into simplified representations. We here refer detailed information about the
 195 processes represented in *ecosys* to the supplement of Grant et al. (2019), and the code of *ecosys*
 196 can be obtained from the online repository (<https://github.com/jinyun1tang/ECOSYS>). Below we
 197 only describe major carbon cycling processes of agroecosystems simulated in *ecosys* (Eq. 1 and
 198 2).

199
$$-NEE = GPP - Reco = GPP - (Ra + Rh) = GPP - ((Rm + Rg) + Rh) \quad (\text{Eq. 1})$$

200
$$NBP = -NEE - Yield - \epsilon \quad (\text{Eq. 2})$$

201 where NEE is net ecosystem exchange, GPP is gross primary production, Ra is ecosystem
 202 autotrophic respiration, Rh is ecosystem heterotrophic respiration, Reco is ecosystem respiration,
 203 Rm and Rg are plant maintenance and growth respiration, NBP is net biome productivity, Yield is
 204 harvested crop yield, and ϵ is the carbon losses caused by disturbances (e.g., fire) excluding harvest.

205 In *ecosys*, the change of SOC (ΔSOC) is equal to the difference between plant litter fall,
 206 Rh, and ecosystem carbon leakage, including CH₄ emission, dissolved organic (DOC) and

207 inorganic carbon (DIC) leaching, etc (Eq. 3a). For annual cropping system in most of the U.S.
 208 Corn Belt regions, we can use NBP to approximate Δ SOC at long term scales (\geq annual scale). By
 209 using Eq. 3, most part of simulated cropland soil carbon balance can be directly backed up with the
 210 eddy covariance measurements or carbon inventory data, which provided another approach to
 211 evaluate and verify the model performance in carbon budget estimations (Baker and Griffis, 2005).

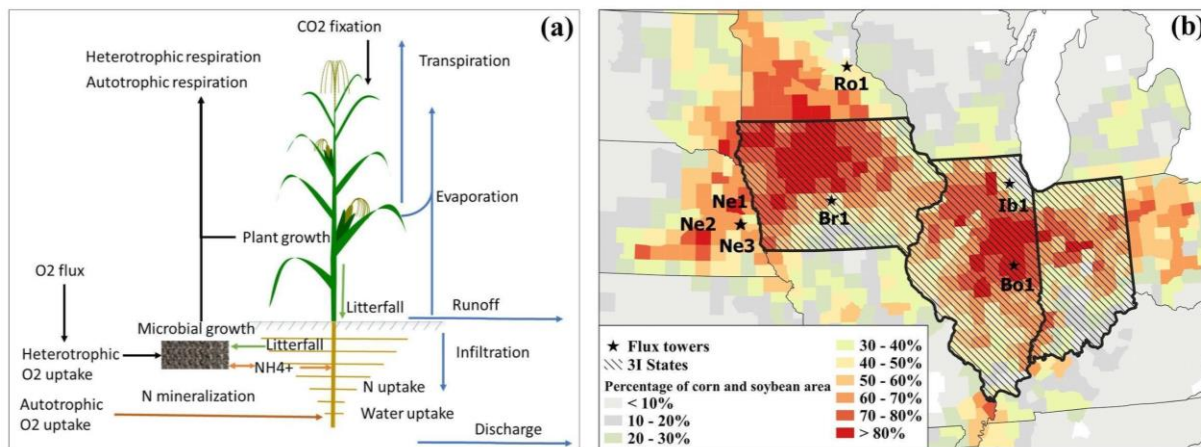
212
$$\Delta\text{SOC} = \text{Litter_Fall} - \text{Rh} - \epsilon \quad (\text{Eq. 3a})$$

213
$$= (\text{GPP} - \text{Ra} - \text{Yield} + \text{Seed_C}) - \text{Rh} - \epsilon \quad (\geq \text{annual scale for annual cropping systems})$$

214
$$= -\text{NEE} + \text{Seed_C} - \text{Yield} - \epsilon = \text{NBP} + \text{Seed_C} - \epsilon \quad (\geq \text{annual scale for annual cropping systems}) \quad (\text{Eq. 3b})$$

215
$$= -\text{NEE} + \text{Seed_C} - \text{Yield} - \epsilon = \text{NBP} + \text{Seed_C} - \epsilon \quad (\geq \text{annual scale for annual cropping systems}) \quad (\text{Eq. 3c})$$

217 where Litter_Fall is the litter fall from plants, including leaf senescence, harvest residue, and root
 218 carbon exudation, Seed_C is the seed mass at planting, ϵ is the carbon leakage through CH₄
 219 emission, and DOC and DIC are leaching terms.



220
 221 **Figure 1.** (a) Major processes represented in the *ecosys* model (revised from (Grant, 2004)), and
 222 (b) locations of the seven flux towers and the three I states in the U.S. Midwest.

223 **2.1.1 Photosynthesis (GPP)**

224 The *ecosys* model uses a multiple-layer canopy module to simulate canopy light absorption
 225 and carbon assimilation (Grant et al., 1989). Photosynthesis of each individual leaf is calculated
 226 independently using the Farquhar model for C3 plants and explicitly considering the mesophyll-
 227 bundle sheath carbon exchange for C4 plants at hourly time step (Farquhar et al., 1980; Grant,
 228 1989a) with specific azimuth, leaf inclination, exposure of light conditions (i.e., sunlit and shaded
 229 leaves), and canopy height. The canopy stomatal resistance (r_c) is controlled by canopy turgor
 230 potential ($\psi_t = \psi_c - \psi_{\pi p}$, where ψ_t , ψ_c , and $\psi_{\pi p}$ represent canopy turgor potential, total water potential
 231 and osmotic potential, respectively) and canopy photosynthesis (Eq. 4) (Grant, 1995; Grant et al.,
 232 1993). ψ_c is calculated through explicitly modeling the plant hydraulics, i.e., by balancing the root
 233 water uptake from different soil layers with that transferred from root to canopy, and transpired
 234 from the canopy to the atmosphere (Grant, 1995). Canopy photosynthesis is calculated by
 235 summing the photosynthesis of all individual leaves, and is coupled with the calculation of canopy
 236 stomatal resistance as:

$$237 \quad r_{cmin} = 0.64 (C_b - C_i') / V_c' \quad r_c \text{ driven by rates of carboxylation vs. diffusion (Eq. 4a)}$$

$$238 \quad r_c = r_{cmin} + (r_{cmax} - r_{cmin}) e^{(-\beta \psi_t)} \quad r_c \text{ constrained by water status (Eq. 4b)}$$

239 where r_c is canopy stomatal resistance to vapor flux, r_{cmin} is the minimum r_c at $\psi_c = 0$ MPa, C_b is
 240 the CO₂ concentration in canopy air, C_i' is the intercellular CO₂ concentration at $\psi_c = 0$ MPa, V_c'
 241 is the potential canopy CO₂ fixation rate at $\psi_c = 0$ MPa, r_{cmax} is canopy cuticular resistance to vapor
 242 flux, and β is the stomatal resistance shape parameter.

243 **2.1.2 Carbon allocation, crop yield, and autotrophic respiration (R_a)**

244 *Ecosys* simulates phenologically-driven plant carbon allocation to shoot and root (Grant,
 245 1989b, 1989c). The dynamic ratio of shoot and root carbon allocation are functions of the number
 246 of phyllochron intervals and of the water and nutrient status of the plant (Grant, 1989b). The

247 allocated carbohydrate will be first used for maintenance respiration (R_m) in both shoot and root,
248 which is calculated based on the canopy temperature (shoot)/soil temperature (root), shoot/root
249 dry biomass, and nutrient stoichiometry. If the allocated carbohydrate can not meet the
250 maintenance respiration, the unmet requirement is remobilized from the existing foliage
251 carbohydrate pool, driving leaf senescence. Remaining carbohydrate after subtracting the
252 maintenance respiration from total carbohydrate is used for growth respiration (R_g) and dry mass
253 (DM) formation. For shoots, DM is partitioned to as many as seven organs, including leaf, sheath,
254 stalk, soluble reserves, husk, cob, and grain, with dynamic partitioning coefficients varying with
255 growth stages (Grant, 1989b). Before floral induction, the shoot DM only consists of leaf and
256 sheath compartments. After floral induction and before anthesis, the shoot DM is allocated to all
257 seven compartments except grain, which begins after anthesis, with partition coefficients
258 calculated from organ growth curves (Grant, 1989b). The modelled yield upon harvest is
259 determined by the seed number and kernel mass set during pre- and post-anthesis growth stages.
260 The plant growth status during stem elongation and the length of post anthesis period together
261 determine the seed number formulation. The kernel mass is determined by the seed growth during
262 the early grain filling stage, limited by the predefined maximum kernel mass (Grant et al., 2011).
263 The grain filling rate in *ecosys* is limited by canopy temperature, and soluble reserve carbon and
264 reserve nutrients in the grain.

265 **2.1.3 Heterotrophic respiration (R_h) and soil carbon dynamics**

266 *Ecosys* computes R_h with explicit microbial dynamics that considers the stoichiometric
267 interactions among carbon, nitrogen and phosphorus (Grant, 2013; Grant and Rochette, 1994).
268 Specifically, organic matter and their transformation occur in five organic matter-microbial
269 complexes, which are coarse woody litter, fine nonwoody litter (including root exudates), animal

270 manure (if applied), particulate organic matter (POM) and humus. Each complex has five organic
271 states, including solid organic matter, sorbed organic matter, microbial residue, dissolved organic
272 matter, and the decomposition agents (microbes), all of which are vertically resolved from the
273 surface litter layer to the bottom of the soil column. The microbes include diverse functional groups,
274 such as obligate aerobes (bacteria and fungi), aerobic and facultative nitrifiers, facultative
275 anaerobes (denitrifiers), obligate anaerobes (fermenters), heterotrophic (acetotrophic) and
276 autotrophic (hydrogenotrophic) methanogens, and aerobic and anaerobic heterotrophic
277 diazotrophs (non-symbiotic N₂ fixers). In computing the organic matter transformation, solid
278 organic matter is first decomposed by microbes as a function of active microbial biomass (as an
279 approximation to the exoenzyme hydrolysis), the product (aka soluble organic matter) is then taken
280 up by microbes in the presence of mineral soil sorption to support microbial catabolic activity (i.e.,
281 heterotrophic respiration), which drives microbial biomass growth and mortality. Mineralization
282 associated with heterotrophic respiration produces ammonium, CO₂ and inorganic phosphorus to
283 drive the metabolism of lithotrophic groups. To maintain the elemental stoichiometry, all microbial
284 groups compete with plants for inorganic nutrients, such as ammonium, nitrate and dissolved
285 inorganic phosphorus. Besides, aerobic microbes also compete with plant roots for oxygen.
286 Therefore, the heterotrophic respiration simulated by *ecosys* comprehensively resolves important
287 process constraints from microbial population dynamics, organic matter formation and
288 destabilization, nutrient limitation and plant-microbial interaction as influenced by the soil
289 physical conditions. Mechanistically, *ecosys* is well positioned to conduct a comprehensive
290 assessment of SOC change and greenhouse gas budget of agroecosystems. More details on the soil
291 biogeochemistry in *ecosys* can be found at Grant (2014).

292 **2.2 Model setup**

293 **2.2.1 Site-scale simulation, calibration, and validation**

294 We evaluated the performance of *ecosys* using seven agricultural sites from the AmeriFlux
295 network (<https://ameriflux.lbl.gov/>) that span a wide range of climate and soil conditions (Figure
296 1b and Table 1) located in the U.S. Midwest. Among these sites, US-Ne1 planted corn during the
297 study period, whereas other sites had corn-soybean rotations; US-Ne1 and US-Ne2 are irrigated
298 sites, whereas other sites are rainfed. Ecosystem CO₂, water, and energy fluxes were measured
299 using the eddy covariance technique at these sites (Baldocchi et al., 2001; Baldocchi, 2003).

300 The hourly gap-filled meteorological variables (i.e., air temperature, precipitation,
301 downward shortwave radiation, humidity, and wind speed) from AmeriFlux and soil information
302 (i.e., bulk density (BD), field capacity (FC), wilting point (WP), soil texture, saturated hydraulic
303 conductivity (KSat), soil organic carbon (SOC), pH, and cation exchange capacity (CEC)) from
304 the Gridded Soil Survey Geographic Database (gSSURGO) at these sites were used to drive *ecosys*.
305 For US-Ne1, US-Ne2 and US-Ne3, detailed land management practices (including planting time
306 and density, irrigation and fertilizer time and amount, tillage time and intensity) from the site
307 records were also available as inputs for the model. For other sites, we used 7.5 plants/m² and 37.1
308 plants/m² for corn and soybean with the planting date from the Risk Management Agency (RMA)
309 of United States Department of Agriculture (USDA) (Lobell et al., 2014), and applied 18g
310 N/m²/year fertilizer before planting for corn years.

311 The time series of GPP, NEE, and Reco of US-Ne1-3 during 2001–2012 were obtained
312 from the FLUXNET2015 Tier 1 dataset (<http://fluxnet.fluxdata.org/data/fluxnet2015-dataset/>),
313 and the LAI and carbon allocation data at different growth stages for those three sites during 2003–
314 2012 were obtained from Carbon Sequestration Program (CSP) at University of Nebraska-
315 Lincoln’s Agricultural Research and Development Center (<http://csp.unl.edu/Public/sites.htm>).

316 For other four sites, the gap-filled GPP, NEE, Reco, and LAI from the AmeriFlux website were
 317 used for the model evaluation. We fine tuned the rubisco carboxylation activity and plant maturity
 318 group parameters of corn and soybean to match the seasonal patterns and magnitude of GPP and
 319 LAI at US-Ne1, US-Ne2 and US-Ne3 sites. The tuned model was evaluated at US-Ne sites using
 320 NEE, Reco, and carbon allocation measurements, and at other sites using the observed GPP, NEE,
 321 Reco, and LAI data.

322

323 **Table 1.** Site information of selected flux towers in the U.S. Midwest for model evaluation.

Site	Latitude	Longitude	MAT (°C)	MAP (mm)	Simulation Period	Site Condition	Crop Types	References
US-Ne1	41.17	-96.48	10.4	710	2001-2012	Irrigated	Continuous corn	(Suyker et al., 2005; Suyker and Verma, 2012; Verma et al., 2005)
US-Ne2	41.16	-96.47	10.4	710	2001-2012	Irrigated	Soybean in even years before 2009, corn in other years	(Suyker et al., 2005; Suyker and Verma, 2012; Verma et al., 2005)
US-Ne3	41.17	-96.44	10.4	710	2001-2012	Rainfed	Corn in odd years and soybean in even years	(Suyker et al., 2005; Suyker and Verma, 2012; Verma et al., 2005)
US-Bo1	40.01	-88.29	11.5	821	2001-2008	Rainfed	Corn in odd years and soybean in even years	(Bernacchi et al., 2005; Meyers, 2004)
US-Br1	41.69	-93.69	9.1	938	2005-2011	Rainfed	Corn in odd years and soybean in	(Hernandez-Ramirez et al., 2011)

							even years	
							Corn in even	
US- Ib1	41.86	-88.22	9.5	972	2005-2011	Rainfed	years and soybean in odd years	(Allison et al., 2005)
							Corn in odd years	
US- Ro1	44.71	-93.09	7.7	764	2004-2012	Rainfed	and soybean in even years	(Baker and Griffis, 2005; Griffis et al., 2008)

324

325 **2.2.2 Regional-scale crop yield and GPP simulation, calibration, and validation**

326 For regional-scale simulations, we focused on the three I states (Illinois, Indiana, and Iowa),
 327 which is the major corn and soybean production area of the U.S. We conducted simulations at each
 328 county within three I states from 2001 to 2018 using corn-soybean rotation without irrigation (the
 329 major planting strategies within this area), using the North American Land Data Assimilation
 330 System (NLDAS-2) hourly meteorological data and gSSURGO soil data as inputs. NLDAS-2
 331 meteorological data is from the integration of observation-based and model reanalysis data, with
 332 0.125° spatial resolution covering central North America. The county scale meteorological
 333 variables were aggregated from the NLDAS-2 grids within that county. The National 2020
 334 Cultivated Layer (based on 2016-2020 USDA Cropland Data Layer) (USDA, 2021) and
 335 gSSURGO datasets were used to obtain the county-scale soil properties (i.e., BD, soil texture, WP,
 336 FC, KSat, SOC, pH, and CEC) that correspond to the county-scale cropland majority soil type.
 337 For regional scale simulations, corn and soybean were also planted with 7.5 plants/m² and 37.1
 338 plants/m² at the county scale based on the RMA planting date (2001–2012) (Lobell et al., 2014)
 339 and the state-scale/agricultural district-scale crop progress reports (2013–2018) depending on the

340 data availability (Figure S4), and all crops were harvested on October 31. The state-wise crop
341 specific fertilizer information provided by USDA (USDA, 2019) was applied in the simulations.

342 For model calibration and evaluation, we used county-scale rainfed corn and soybean yield
343 from USDA National Agricultural Statistics Service (NASS), and a new 250m resolution daily
344 GPP estimation using MODIS-based soil-adjusted near-infrared reflectance of vegetation
345 (SANIRv) and photosynthetically active radiation (PAR) (Jiang et al., 2021). The fixed linear yield
346 trend was calculated from the NASS crop yield data for corn and soybean respectively for each
347 county, and was used to adjust the simulated yield to year 2009 (the midpoint of 2001-2018). To
348 constrain *ecosys* efficiently, we built the surrogate models for crop yield and GPP separately using
349 the Long Short Term Memory networks (LSTM) to predict daily GPP and end-of-seasonal crop
350 yield under different corn and soybean parameters. In these models, the daily climate
351 meteorological data, three layers soil parameters (i.e., 0-5, 5-30, and 30-100cm), crop type, corn
352 parameters, soybean parameters, fertilizer amount, planting and harvest date, and day of year
353 (DOY) were used as input, and GPP or crop yield were used as output, respectively. The RMSE
354 of the surrogate models are 13.5 gC/m^2 and $0.46 \text{ gC/m}^2/\text{day}$ for yield and GPP, respectively. The
355 parameters for soybean include rubisco carboxylation activity, plant maturity group, maximum
356 number of fruiting sites per reproductive node, and maximum rate of kernel filling, and for corn
357 include fraction of leaf protein in bundle sheath chlorophyll, plant maturity group, maximum
358 number of fruiting sites per reproductive node, and maximum rate of kernel filling. We conducted
359 the parameter calibration for each county based on the surrogate models, and used data from even
360 years during 2001 to 2018 for model constraint and those from odd years for model validation. In
361 applying the constraint, the difference between simulated and observed yield, accumulated

362 growing season (i.e., May to September) GPP, and monthly growing season GPP were minimized
 363 using the cost function in Eq. 5c.

$$364 \quad L(\text{soybean}) = NRMSE_{\text{yield}}(\text{soybean}) + NRMSE_{GPP}(\text{soybean}) + NRMSE_{GPP_monthly}(\text{soybean}) \quad (\text{Eq. 5a})$$

$$365 \quad L(\text{corn}) = NRMSE_{\text{yield}}(\text{corn}) + NRMSE_{GPP}(\text{corn}) + NRMSE_{GPP_monthly}(\text{corn}) \quad (\text{Eq. 5b})$$

$$366 \quad L = L(\text{soybean}) + L(\text{corn}) \quad (\text{Eq. 5c})$$

367 where $NRMSE_{\text{yield}}(\text{soybean})$ and $NRMSE_{\text{yield}}(\text{corn})$ are normalized RMSE of model simulated and
 368 measured crop yield for corn and soybean, respectively based on Eq. 6; $NRMSE_{GPP}(\text{soybean})$ and
 369 $NRMSE_{GPP}(\text{corn})$ are normalized RMSE of model simulated and measured growing season
 370 accumulated GPP for corn and soybean, respectively based on Eq. 7; $NRMSE_{GPP_monthly}(\text{soybean})$
 371 and $NRMSE_{GPP_monthly}(\text{corn})$ are normalized RMSE of model simulated and measured growing
 372 season monthly GPP for corn and soybean, respectively based on Eq. 8.

$$373 \quad NRMSE_{\text{yield}} = \frac{\sqrt{\frac{1}{9} \sum_{\text{year}=\text{even_years}} (\text{Yield}_{\text{sim}}(\text{year}) - \text{Yield}_{\text{obs}}(\text{year}))^2}}{\frac{1}{9} \sum_{\text{year}=\text{even_years}} \text{Yield}_{\text{obs}}(\text{year})} \quad (\text{Eq. 6})$$

$$374 \quad NRMSE_{GPP} = \frac{\sqrt{\frac{1}{9} \sum_{\text{year}=\text{even_years}} (\text{GPP}_{\text{sim}}(\text{year}) - \text{GPP}_{\text{obs}}(\text{year}))^2}}{\frac{1}{9} \sum_{\text{year}=\text{even_years}} \text{GPP}_{\text{obs}}(\text{year})} \quad (\text{Eq. 7})$$

$$375 \quad NRMSE_{GPP_monthly} = \frac{\sqrt{\frac{1}{5} \sum_{\text{month}=5} \left(\frac{\sum_{\text{year}=\text{even_years}} \text{GPP}_{\text{sim}}(\text{year}, \text{month})}{9} - \frac{\sum_{\text{year}=\text{even_years}} \text{GPP}_{\text{obs}}(\text{year}, \text{month})}{9} \right)^2}}{\frac{1}{45} \sum_{\text{year}=\text{even_years}} \sum_{\text{month}=5} \text{GPP}_{\text{obs}}(\text{year}, \text{month})}} \quad (\text{Eq. 8})$$

376 where $\text{Yield}_{\text{sim}}(\text{year})$ and $\text{Yield}_{\text{obs}}(\text{year})$ are the simulated and observed yield, $\text{GPP}_{\text{sim}}(\text{year})$ and
 377 $\text{GPP}_{\text{obs}}(\text{year})$ are the simulated and observed growing season accumulated GPP, $\text{GPP}_{\text{sim}}(\text{year}, \text{month})$ and
 378 $\text{GPP}_{\text{obs}}(\text{year}, \text{month})$ are the simulated and observed GPP at certain month, *even_years* is the years used
 379 for model constrain (i.e., 2002, 2004, ..., 2018).

380

381

382

383 3. Results

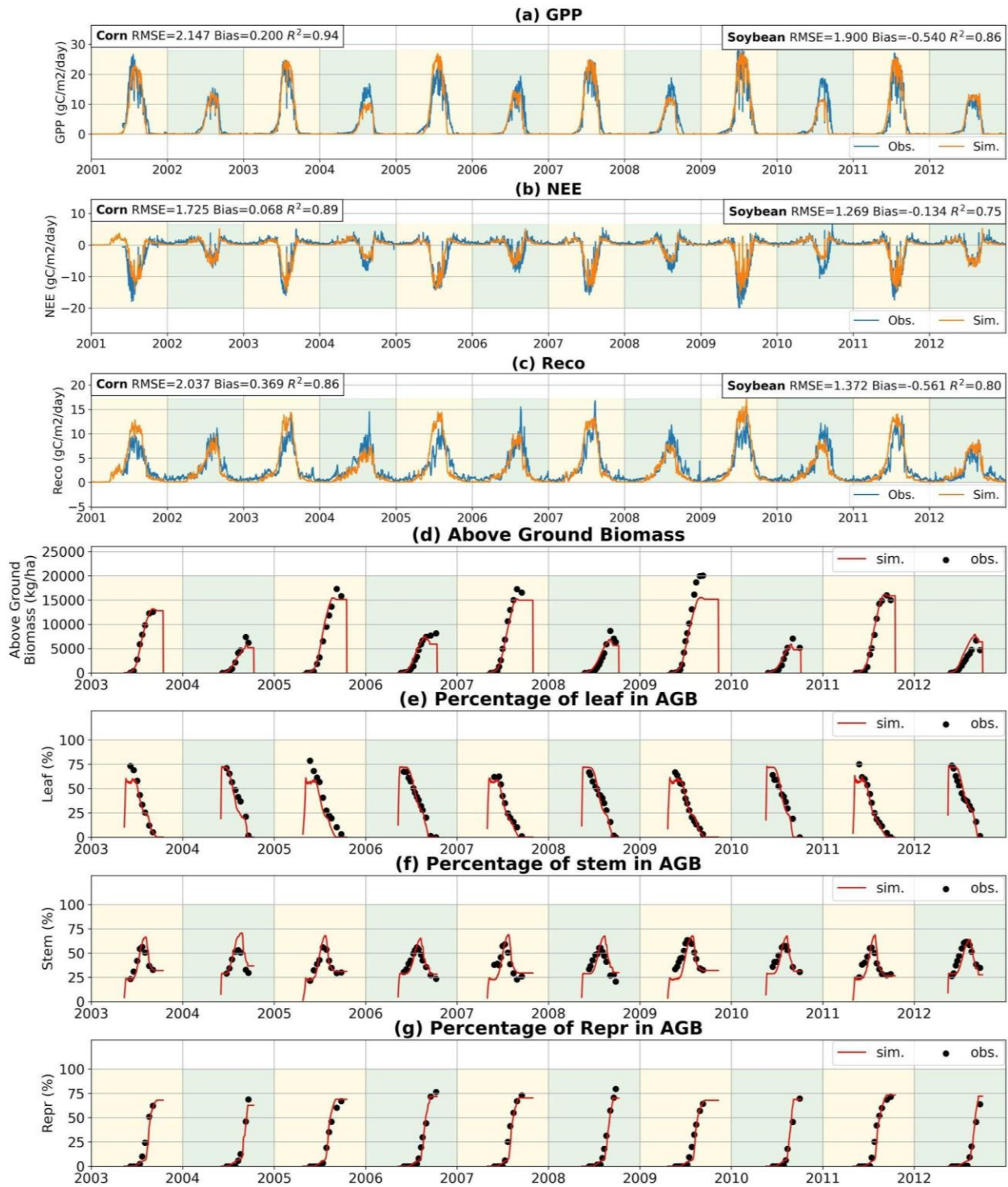
384 3.1 Site-scale validation of *ecosys* in simulating carbon dynamics

385 We compared observed and modelled GPP, NEE, Reco fluxes at 7 eddy-covariance sites
386 in the U.S. Midwest (Figure 1b). The results indicate that *ecosys* can capture both the magnitude
387 and seasonal patterns of these carbon fluxes with high accuracy at both daily and monthly scale
388 (i.e., Figure 2, 3, S1, S2, and Table 2). The simulated GPP is consistent with the observations for
389 both corn and soybean throughout the growing season, and can reflect the magnitude difference
390 between corn and soybean during peak growing season. At the daily scale, R^2 and RMSE are 0.94
391 and 2.15 gC/m²/day for corn, and are 0.86 and 1.90 gC/m²/day for soybean at Ne3, respectively
392 (Figure 2a). The seasonal pattern and magnitude of Reco, which is high during summer and low
393 during winter in the U.S. Midwest, can be captured by *ecosys* for both corn and soybean with high
394 modeling skills (i.e., $R^2=0.86$ and RMSE=2.04 gC/m²/day for corn, and $R^2=0.80$ and RMSE=1.37
395 gC/m²/day for soybean at Ne3, Figure 2c). As for NEE, the magnitude, peaking time, and zero-
396 crossing points in observations are all captured by *ecosys* with $R^2=0.89$ and RMSE=1.73
397 gC/m²/day for corn, and $R^2=0.75$ and RMSE=1.27 gC/m²/day for soybean, respectively, at Ne3
398 (Figure 2b).

399 The comparison of observed and modelled above ground biomass (AGB) and its partition
400 showed that the dynamics of AGB and its allocation to leaf, stem, and reproductive organs can be
401 reproduced by *ecosys* for both corn and soybean, ensuring the application of *ecosys* for crop yield
402 simulation (Figure 2, S1, and S2). The R^2 between the measured and simulated AGB and its leaf,
403 stem, and reproductive percentages are 0.95, 0.92, 0.60, and 0.94 at Ne3. In both observations and
404 simulations, during the early growing season, the AGB increase appears mostly as leaves to
405 increase photosynthesis; during the peak growing season, the AGB increase is mostly found in

406 stem for plant structural support, and at the late stage, the AGB increase is mostly allocated to the
407 reproductive organ for grain formulation.

408 We also compared the responses of the modelled and observed GPP, Reco, and NEE to the
409 air temperature (T_a) and vapor pressure deficit (VPD) at those eddy-covariance sites (Figure 4 and
410 S3). The results indicate that *ecosys* captured the responses of major carbon fluxes e.g. GPP, Reco
411 and NEE to variations in air temperature and VPD at the eddy-covariance sites reasonably well.
412 Taking corn as an example, when T_a is less than 30°C, GPP increases quickly, but stays stable
413 when T_a becomes higher. Both observations and simulations show such a response, which is
414 primarily controlled by the limitation of temperature on leaf rubisco activity. As for the response
415 of GPP to VPD, GPP increases when VPD is small, but decreases when VPD gets higher in both
416 observations and simulations, which reveals the emergent influence of VPD on crop stomatal
417 conductance. The observed Reco showed a strong response to T_a (i.e., increases quickly with
418 higher T_a when T_a is below the optimal value) and no significant response to VPD, which can also
419 be captured by the *ecosys* simulations. As for NEE, the balance of carbon fixation and respiration
420 shows similar responses to T_a and VPD as that of GPP in both observations and simulations. The
421 reason that results in the similar response of NEE and GPP to environmental factors is that NEE
422 is dominated by crop photosynthesis during peak growing season. Similar responses of GPP, NEE,
423 and Reco to T_a and VPD are also captured by *ecosys* simulations for soybean at the eddy-
424 covariance sites (i.e., Figure S3).

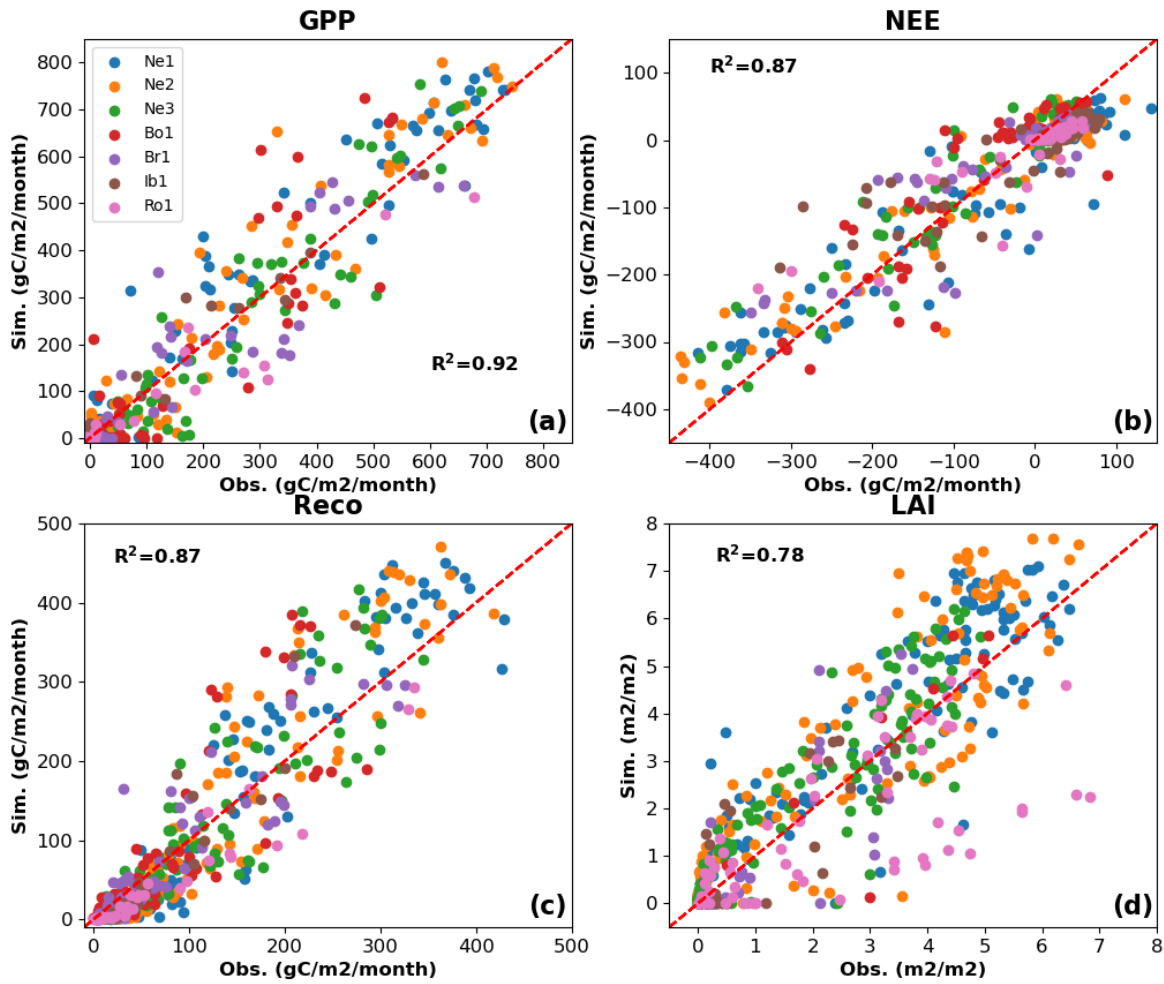


425

426 **Figure 2.** Comparing *ecosys* simulated GPP, NEE, Reco and carbon allocation with site

427 observations at Mead Ne3 site in Nebraska for both corn (light yellow shaded) and soybean (light

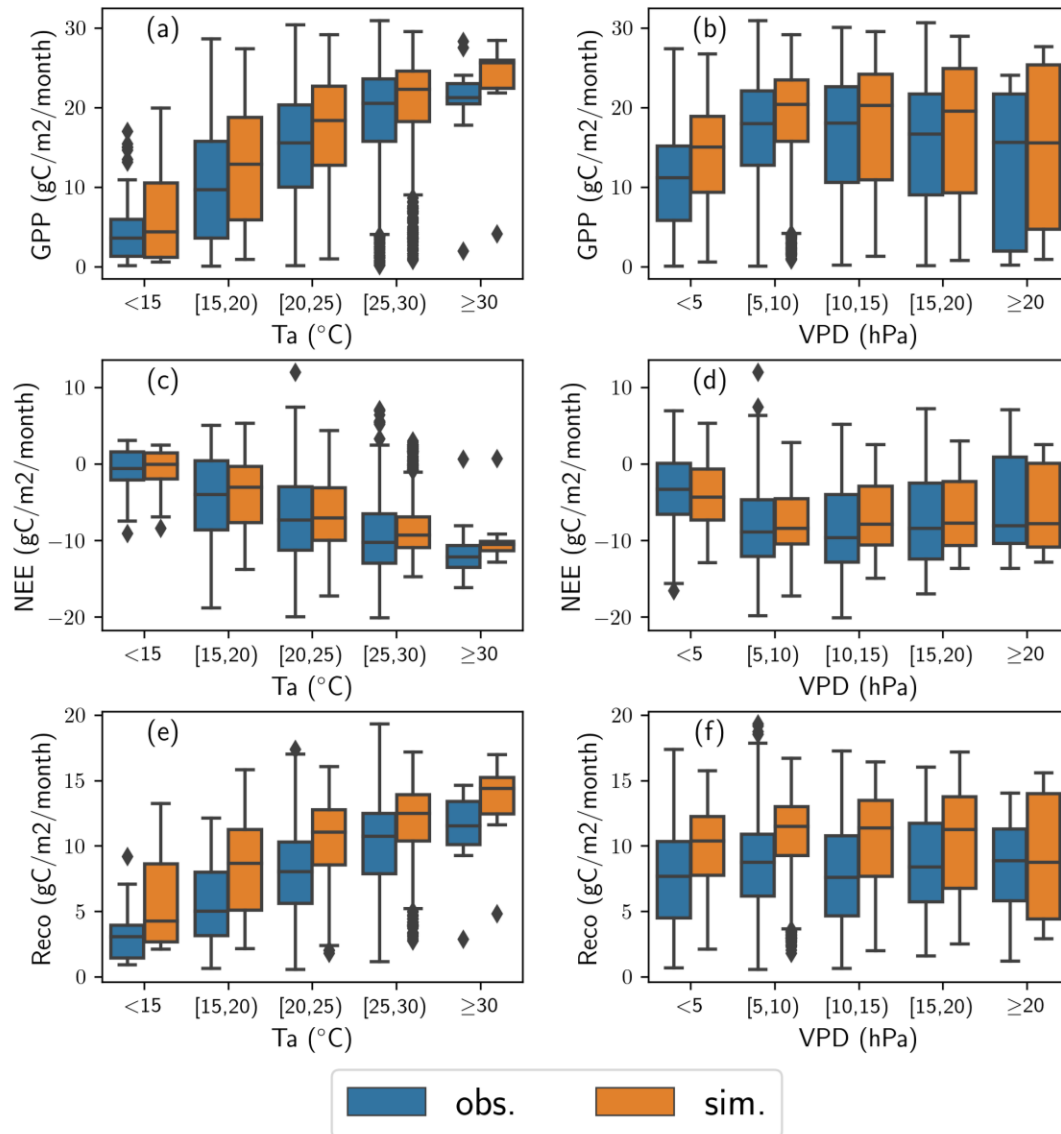
428 blue shaded).



429

430 **Figure 3.** Comparison of simulated and observed carbon fluxes (monthly) and LAI at the flux
 431 tower sites. Red dashed lines indicate the 1-to-1 line.

Corn



432

433 **Figure 4.** Responses of simulated and observed daily GPP, NEE, and Reco to air temperature and
 434 VPD for corn during peak growing season (June to August).

435

436

437

438

439 **Table 2.** Comparison statistics of *ecosys* simulated daily surface carbon fluxes with flux towers
 440 observations.

Sites	NEE			GPP			Reco		
	RMSE (gC/m ² /day)	Bias (gC/m ² /day)	R ²	RMSE (gC/m ² /day)	Bias (gC/m ² /day)	R ²	RMSE (gC/m ² /day)	Bias (gC/m ² /day)	R ²
Ne1	1.96	-0.60	0.86	2.44	0.67	0.93	1.92	-0.07	0.87
Ne2	1.67	-0.28	0.88	2.32	0.25	0.92	1.98	-0.03	0.83
Ne3	1.51	-0.04	0.86	2.02	-0.18	0.91	1.72	-0.11	0.79
Bo1	2.26	0.11	0.65	3.31	0.06	0.74	2.04	0.21	0.67
Br1	2.34	0.04	0.59	2.66	-0.06	0.80	1.46	-0.01	0.77
Ib1	1.90	-0.35	0.69	1.64	0.28	0.91	1.66	0.05	0.77
Ro1	1.77	-0.15	0.69	2.12	-0.69	0.89	1.30	-0.78	0.89

441

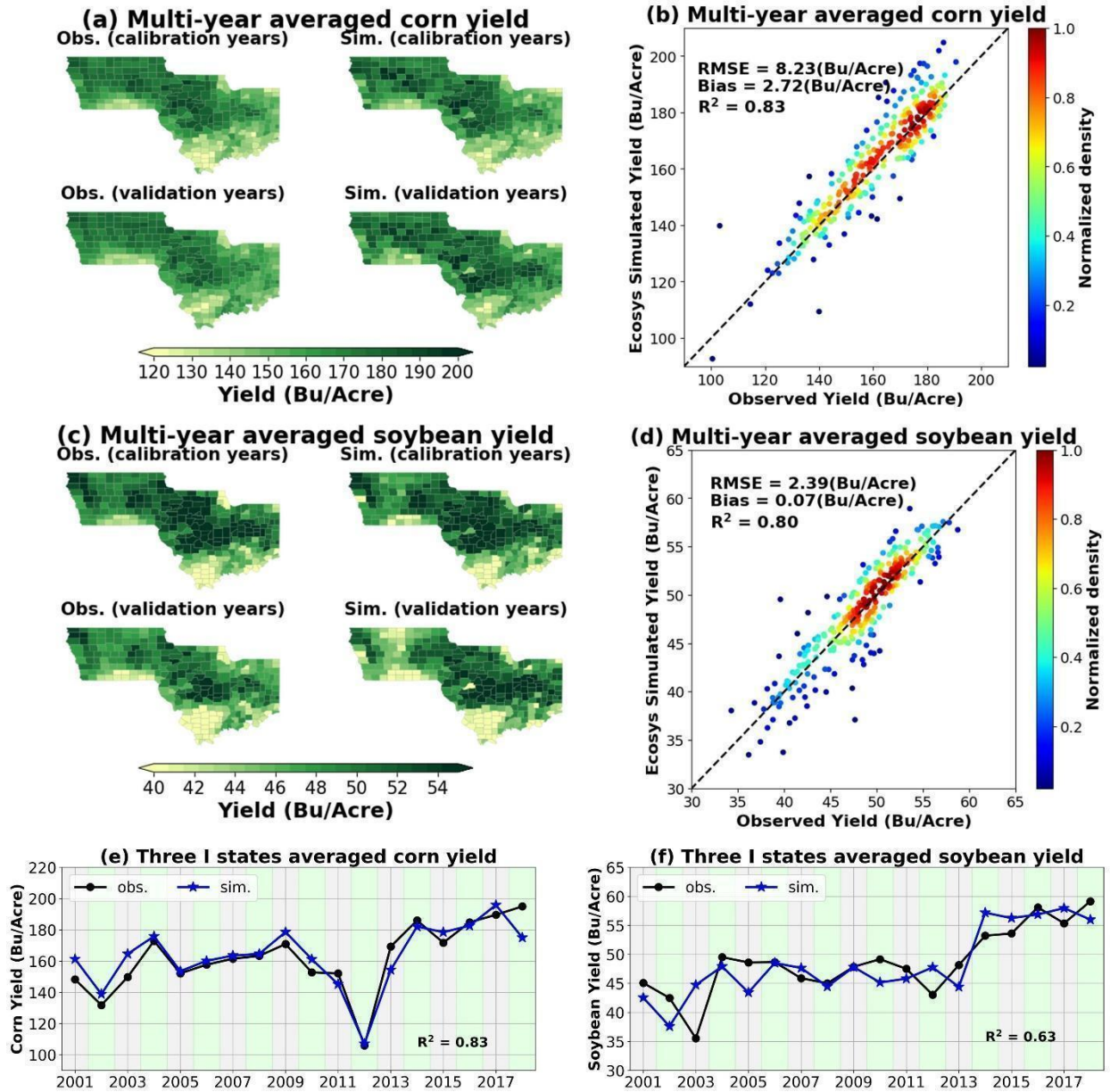
442 **3.2 Regional-scale crop yield and gross primary productivity simulation**

443 **3.2.1 Regional-scale corn and soybean yield simulation**

444 The comparison between modelled and NASS reported crop yield shows that *ecosys* can
 445 reproduce the spatial distribution and interannual variability of crop yield over three I States for
 446 both corn and soybean (Figure 5, Figure S5-7). Modeled long-term (2001–2018) averaged crop
 447 yield and NASS ground truth shows similar spatial patterns over three I States during both
 448 calibration years and validation years for both corn and soybean. The R², RMSE, and bias between
 449 the spatial patterns of modelled and measured yield are 0.83, 8.23 Bu/Acre, and 2.72 Bu/Acre for
 450 corn, and 0.80, 2.39 Bu/Acre, and 0.07 Bu/Acre for soybean, respectively. Long-term averaged

451 corn and soybean yield in the northern part of three I States are higher than that of the southern part
452 in both observations and simulations, which may be caused by the differences in soil (i.e., higher
453 SOC in the northern part) and climate conditions (i.e., more frequent heat stress and extreme
454 precipitation events in the southern part). The temporal variation of simulated average yield during
455 2001 to 2018 is also consistent with the observations with R^2 of 0.83 and 0.63 for corn and soybean,
456 respectively.

457



458

459 **Figure 5.** Comparison of *ecosys* simulated crop yield and NASS reported crop yield. (a) Spatial
 460 patterns of simulated and observed multi-year averaged corn yield in calibration and validation
 461 years. (b) Density scatter plot of simulated and observed multi-year averaged corn yield. Different
 462 colors mean different normalized density (means the ratio of points density to maximum points
 463 density, similar for the density scatter plot in other figures). (c) Spatial patterns of simulated and
 464 observed multi-year averaged soybean yield in calibration and validation years. (d) Density scatter

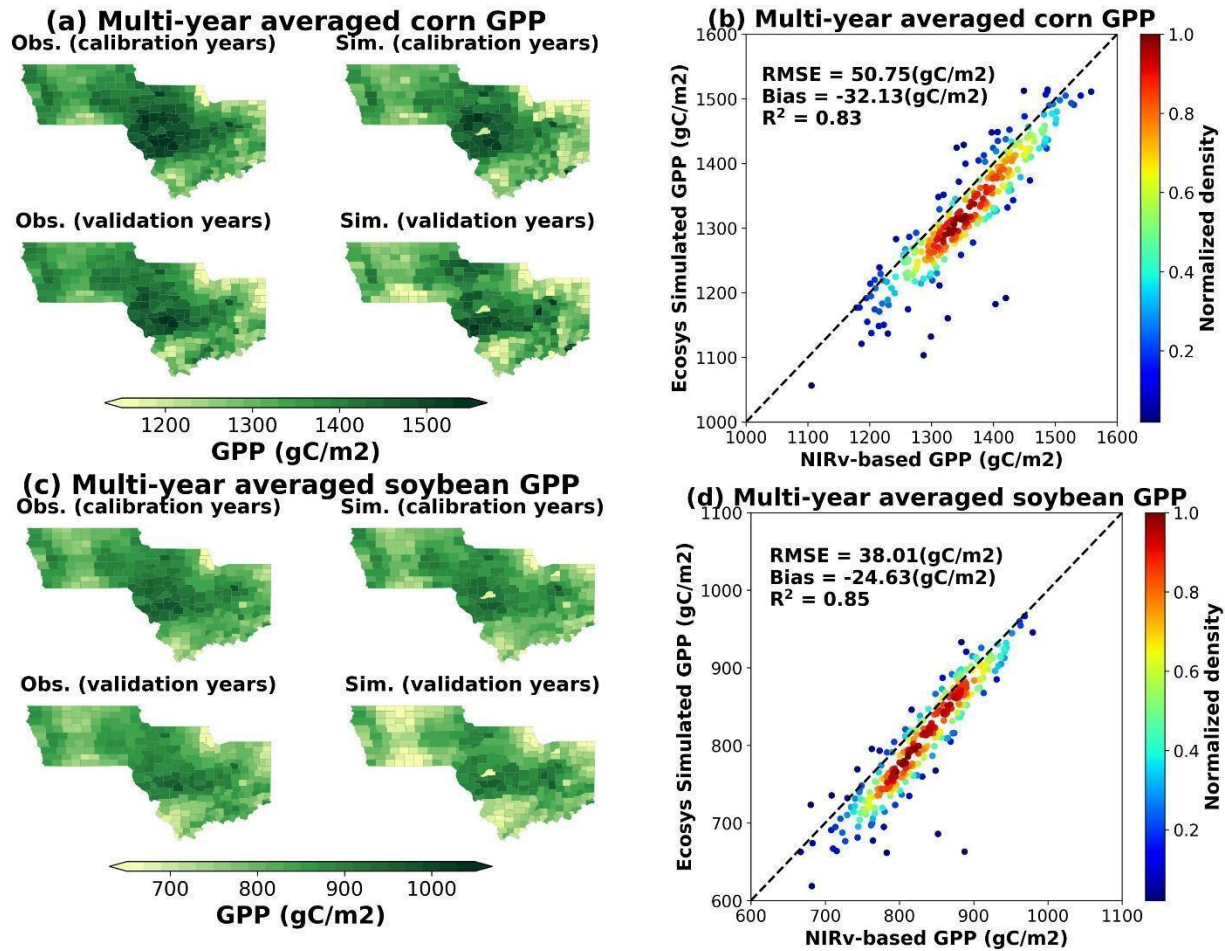
465 plot of simulated and observed multi-year averaged soybean yield. (e) and (f) is the time series of
466 three I states averaged corn and soybean yield respectively. Light green shaded years in (e) and (f)
467 are calibration years, and grey shaded years are validation years.

468

469 **3.2.2 Regional-scale corn and soybean GPP simulation**

470 We also compared the modeled long-term averaged GPP and a new satellite-based GPP
471 estimation during the peak growing season (June to August). The spatial patterns of simulated and
472 NIRv-based peak growing season accumulated GPP are similar during calibration years and
473 validation years for both corn and soybean (Figure 6), which are consistent with the spatial patterns
474 of yield (Figure 5). The R^2 , relative RMSE between the spatial patterns of modelled and NIRv-
475 based GPP are 0.83 and 3.7% for corn, and 0.85 and 4.6% for soybean, respectively. The seasonal
476 variation of GPP for both corn and soybean can also be captured by *ecosys* at regional scale when
477 benchmarked with NIRv-based GPP (Figure 7, Figure S8, S10). For example, GPP of corn and
478 soybean grows quickly from June to July, and peaks at July and August in both simulations and
479 NIRv-based observations (Figure 7).

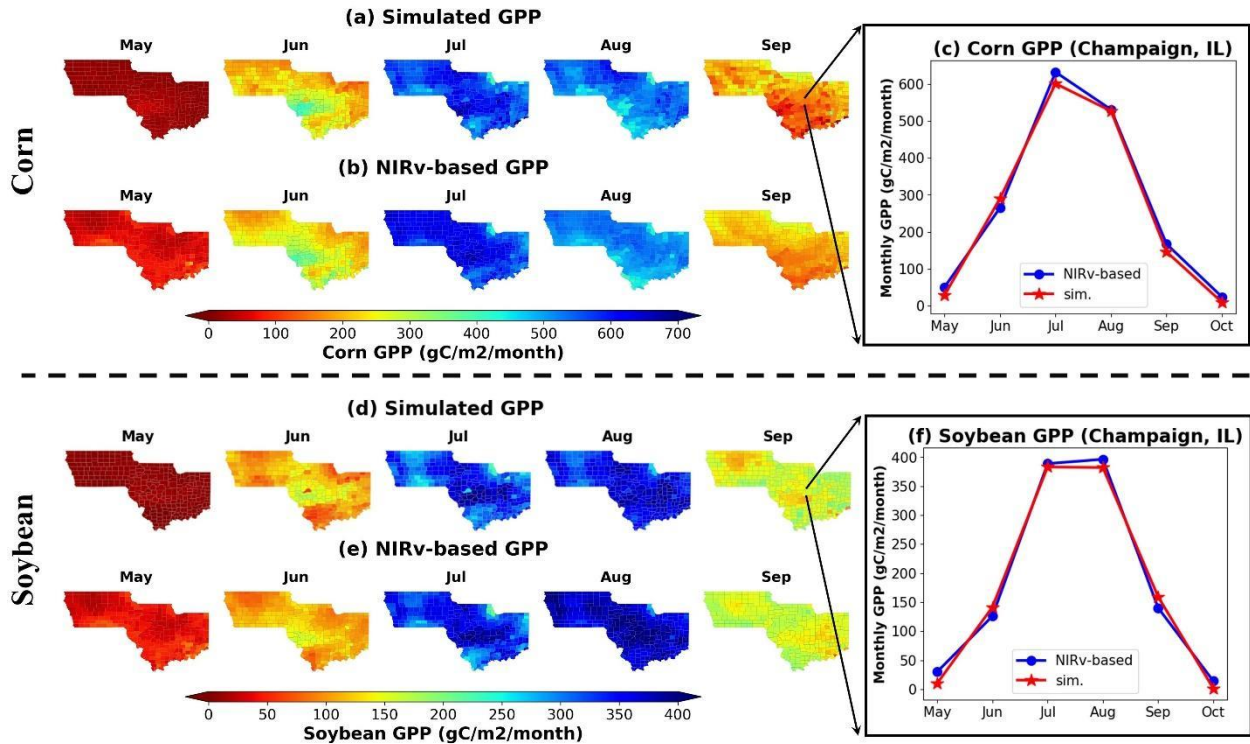
480



481

482 **Figure 6.** Comparison of *ecosys* simulated peak growing season accumulated (June to August)
 483 GPP and NIRv-based GPP. (a) Spatial patterns of simulated and NIRv-based multi-year averaged
 484 corn GPP in calibration and validation years. (b) Density scatter plot of simulated and NIRv-based
 485 multi-year averaged corn GPP. (c) Spatial patterns of simulated and NIRv-based multi-year
 486 averaged soybean GPP in calibration and validation years. (d) Density scatter plot of simulated
 487 and NIRv-based multi-year average soybean GPP.

488



489

490 **Figure 7.** Comparison of multi-year averaged *ecosys* simulated and NIRv-based monthly GPP for
 491 corn and soybean in validation years. (a) Simulated multi-year averaged monthly corn GPP during
 492 validation years. (b) NIRv-based multi-year averaged monthly corn GPP during validation years.
 493 (c) Comparison of simulated and NIRv-based multi-year averaged monthly corn GPP at
 494 Champaign, IL during validation years. (d) Simulated multi-year averaged monthly soybean GPP
 495 during validation years. (b) NIRv-based multi-year averaged monthly soybean GPP during
 496 validation years. (c) Comparison of simulated and NIRv-based multi-year averaged monthly
 497 soybean GPP at Champaign, IL during validation years.

498

499 3.3 Response of crop yield to environmental variability in the U.S. Midwest

500

501

502

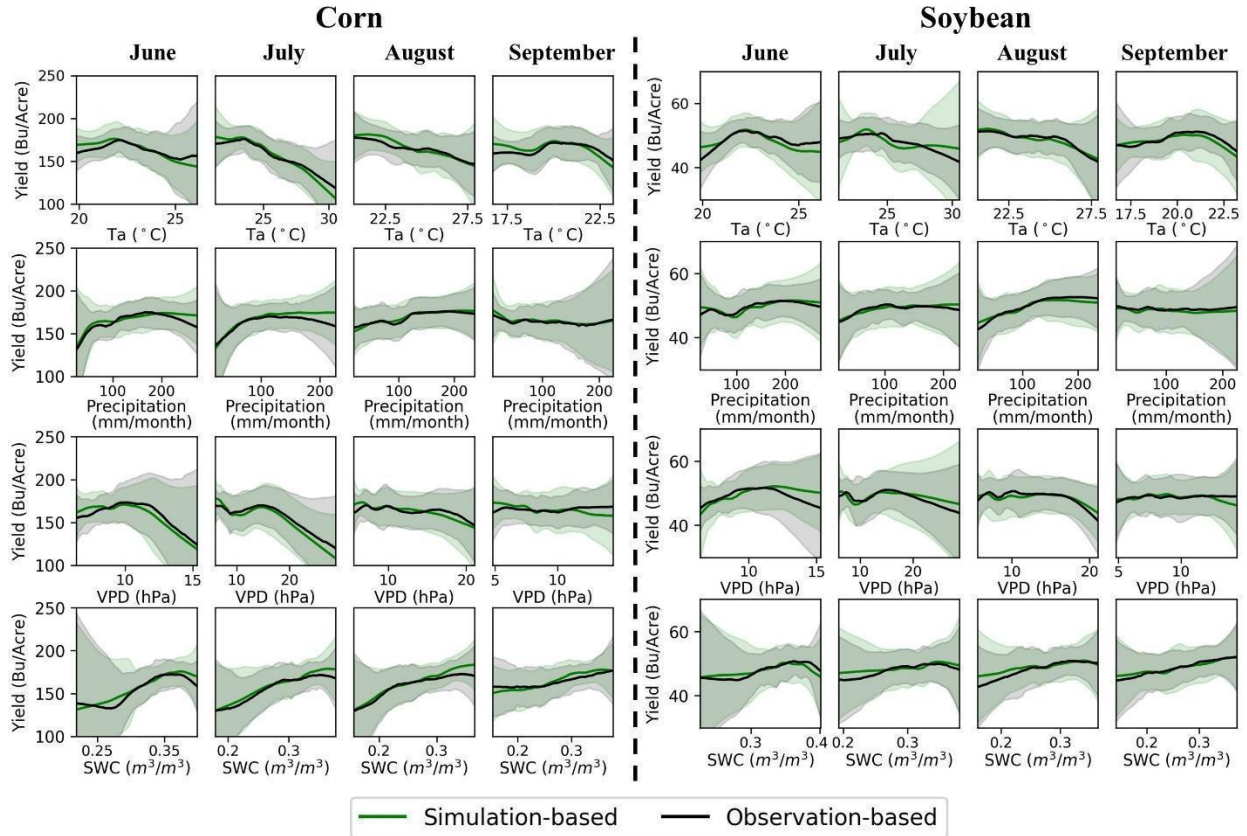
Besides comparing the absolute value of modelled and observed yield and GPP, we also investigated the response of these variables to the environmental factors to evaluate whether the model could capture such response (Figure 8, Figure 9, and Figure S12). The LOWESS (LOcally

503 Weighted Scatterplot Smoothing) was used to fit the response of observed and modelled crop yield
504 to key environmental factors, including Ta, precipitation , VPD, soil water content (SWC), bulk
505 density, and SOC, in the U.S. Midwest for corn and soybean during the growing season (Figure
506 8).

507 We found that the trend and inflection points of the observation-based response curves can
508 be simulated by *ecosys* at the regional scale for most of the months for climate variables and
509 different depths for soil properties, demonstrating the ability of *ecosys* in capturing the response
510 of crop yield to environmental variabilities in the U.S. Midwest. Both observations and simulations
511 show that yield increases with increasing Ta until an optimal Ta value, and then decreases with
512 higher Ta. The yield~Ta response is caused by the plant enzyme and growth activity with
513 temperature, which is also reflected in the GPP~Ta response (Figure S12) during key growing
514 months (i.e., July and August). For precipitation, the yield increases with increasing precipitation
515 when precipitation is smaller and then decreases at higher precipitation, revealing the tradeoff
516 between water limitation and excessive precipitation on crop growth (Li et al., 2019). For VPD,
517 the yield increases with VPD when VPD is low, and decreases when VPD is higher, confirming
518 the impacts of VPD on crop productivity in both photosynthesis (through the VPD control on
519 stomatal conductance) (Ball, 1988; Grant et al., 1993) and crop yield (Kimm et al., 2020; Lobell
520 et al., 2014; Zhou et al., 2020). The response of yield~SWC is similar to other environmental
521 variables, revealing the tradeoff between water supply and oxygen stress at high soil moisture on
522 crop growth. For both observations and simulations, the multi-year averaged crop yield decreases
523 with larger bulk density and increases with larger SOC in the U.S. Midwest.

524

525



526

527 **Figure 8.** Fitted responses of *ecosys* simulated and observed crop yield to climate variables at three
 528 I States for corn and soybean using LOWESS. The shaded regions are the 95% confidence intervals
 529 of LOWESS.

530

531

532

533

546 we tested *ecosys* performance at seven majority cropland eddy-covariance sites (with 55 site-years
547 observations) across the U.S. Midwest regarding GPP, NEE, Reco, LAI, and carbon allocation.
548 The model validation results reveal that *ecosys* can simulate the seasonal cycle and magnitude of
549 agroecosystem carbon dynamics at different individual sites with high accuracy. Across all the
550 sites, the R^2 of the simulated and observed value for GPP, NEE, Reco, and LAI were 0.92, 0.87,
551 0.87, and 0.78, respectively (Figure 3). In addition, the dynamics of above ground biomass and its
552 allocation to leaf, stem, and reproductive can be reproduced by *ecosys* (Figure 3, S1, and S2). The
553 overall model performance at Ne1, Ne2, and Ne3 sites are better than that at the other 4 sites in
554 simulating GPP, NEE and Reco (Table 2), which may largely be attributed to the more accurate
555 records of land management practice (i.e., planting date and planting density, tillage information,
556 and irrigation information) at the Mead Ne sites.

557 Since the crop cultivar (e.g., maturity group) and management practices (e.g., fertilizer rate,
558 planting date) may varies in spatial, and is hard to obtain the information at high resolution, we
559 calibrated the *ecosys* model using the existing observations from both USDA survey for yield and
560 satellite-based novel GPP estimations in even years to take the spatial variation of cultivars and
561 management practices into account, and validated the model in odd years at the regional scale by
562 simulating over 293 counties in the three I States. The model validation results show that *ecosys*
563 can capture the spatial and temporal variability of crop yield as well as the magnitude and seasonal
564 patterns of GPP for both corn and soybean across the broader regions in the U.S. Midwest. The R^2
565 of the multi-year averaged simulated and observed yield for corn and soybean is 0.83 and 0.80,
566 respectively, showing the advanced ability of *ecosys* in capturing the crop yield spatial variance.
567 Based on our best knowledge, such a high performance in simulating crop yield with a direct
568 benchmark with county-level NASS data has not been achieved before (Zhang et al., 2015, 2020),

569 which is a strong demonstration of the ability of *ecosys* in simulating the carbon cycle for
570 agroecosystems. The interannual variability of the observed crop yield can also be matched by
571 *ecosys* simulations, but with some deviations at some years (i.e., 2003) between the observations
572 and simulations for soybean, which may be caused by abiotic stress, such as pest, diseases, or
573 uncaptured environmental impacts (e.g. hail, wind storm).

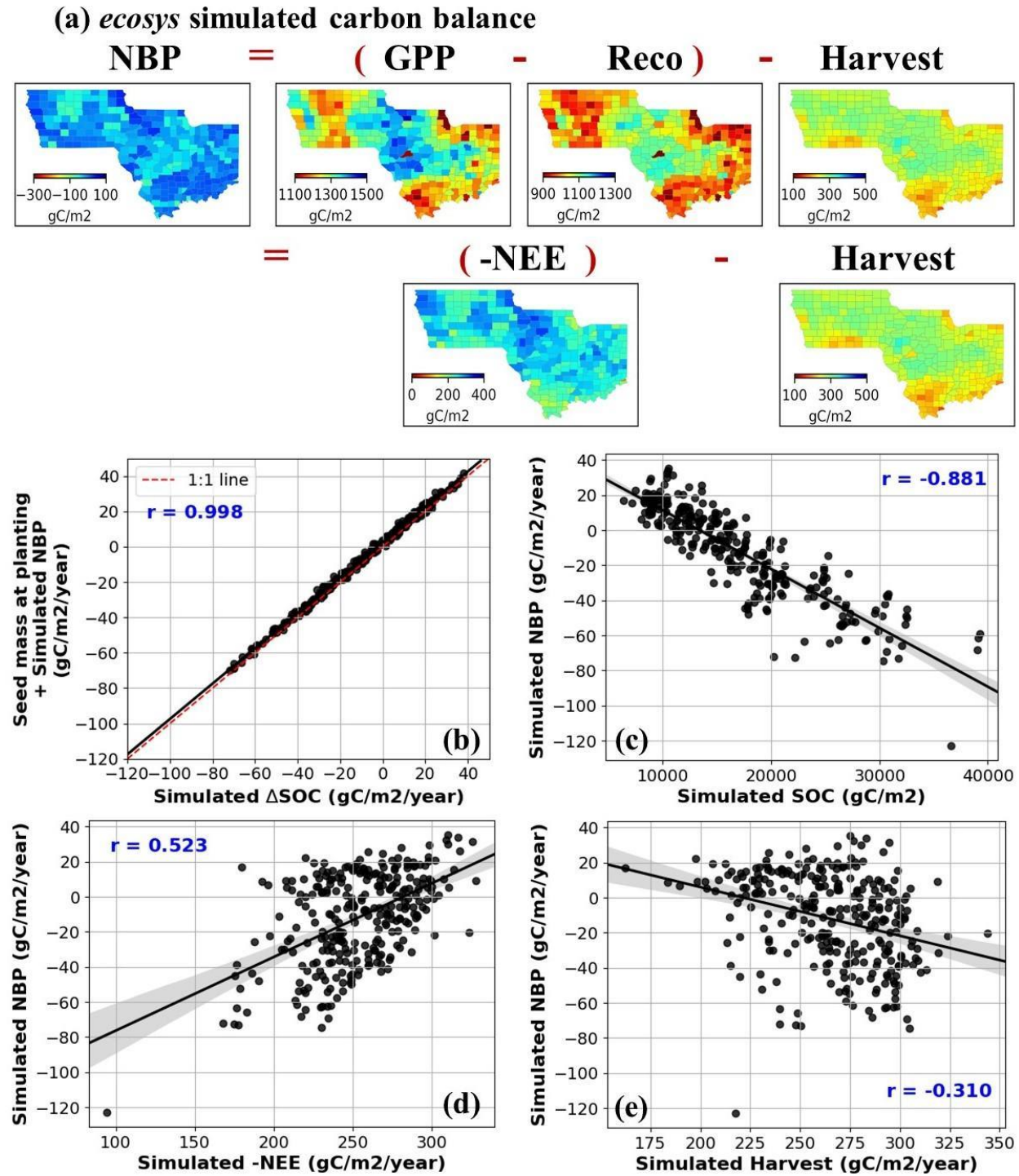
574 To fill the gap that previous studies only focused on matching the magnitude of the
575 simulated target variables with observations, we also corroborated the simulated and observed
576 responses of carbon-related variables to climate and soil variabilities in both the site scale and
577 regional scale simulations. The response of the carbon flux and crop yield to the environmental
578 variabilities obtained from the observations can be captured well by *ecosys*. For the site scale
579 simulation, the responses of the modelled and observed GPP, Reco, and NEE to the ambient
580 climate conditions (i.e., temperature and VPD) at the eddy-covariance sites are consistent; For the
581 regional scale simulations, the responses of simulated crop yield/GPP to the environmental factors
582 were similar to those of the observations during the growing season (i.e., Figure 8, Figure 9, and
583 Figure S12). These results indicate the ability of *ecosys* in simulating carbon fluxes and crop yield
584 across the border soil and weather conditions.

585 Through the comprehensive evaluation of the simulated carbon components with the
586 observations (including GPP, Reco, and carbon allocation at eddy-covariance sites, and GPP and
587 yield at regional scales), we are able to simulate the NBP at the regional scale (Figure 10). The
588 simulated multi-year averaged NBP had higher negative correlation to the SOC and NEE in the
589 same period with r of -0.88 and -0.52, respectively, which indicates that both SOC stock and NEE
590 drives NBP dynamics across space. As indicated in Eq. 3, annually, the accumulated NBP is
591 approximately equal to ΔSOC , assuming ε (carbon leakage through runoff and methane emission)

592 is sufficiently small. Our simulation results confirmed that using the carbon mass balance approach,
593 we can regiously predict Δ SOC (Figure 10b). This means that our method has the potential to be
594 applied for quantifying annual-scale soil carbon sequestration for agroecosystems. However,
595 cautions are given that, in being able to ensure the carbon mass balance approach work or have a
596 low uncertainty, rigorous tests of different carbon cycle components, i.e., GPP, Reco, and harvest
597 carbon, all should be conducted - currently no existing modeling-based study has demonstrated
598 such a capability except this current study.

599

600



601

602 **Figure 10.** Simulated multi-year averaged corn-soybean rotation cropland NBP during 2001-2018,

603 and its correlation with ΔSOC , SOC content, NEE, and harvest over three I states. (a) Simulated

604 multi-year averaged corn-soybean rotation cropland carbon budget over three I states during 2001

605 to 2018. (b) The scatter plot of simulated SOC change and the sum of seed mass at planting and
606 NBP. (c) The scatter plot of averaged simulated SOC and NBP. (d) The scatter plot of simulated
607 NEE and NBP. (e) The scatter plot of simulated harvest carbon and NBP. The black lines and
608 shaded regions in (b)-(e) are the fitted linear regression models and the corresponding 95%
609 confidence interval.

610 Although we had validated the ability of *ecosys* in simulating the carbon cycle processes
611 for both crop yield and GPP, there are still some limitations in the regional scale carbon balance
612 simulation that need to be further addressed. Specifically, in current simulations, we only focus on
613 the case that with no tillage and no cover crop. In the U.S. Midwest, tillage and cover crop are the
614 commonly adopted conservation practices (Deines et al., 2019; Seifert et al., 2019), and may
615 change the soil carbon sequestration rate compared with the no till and no cover crop situation
616 (Baker et al., 2007; Poeplau and Don, 2015). For the tillage practice, it may redistribute SOC
617 content in the soil profile, affect the crop growth by influencing soil minimization and soil water
618 content, and also affect ecosystem respiration especially R_h (Mehra et al., 2018). For cover crops,
619 it may influence the SOC sequestration rate by increasing GPP in the winter period and competing
620 the water and nutrients with the main crops in the summer (Abdalla et al., 2019). Studying the
621 impacts of cover crop and tillage is beyond the scope of the current paper, but they are under active
622 investigation in our other studies.

623

624 **5. Conclusion**

625 In conclusion, we evaluated an advanced agroecosystem model, *ecosys*, to thoroughly
626 simulate carbon budget for the agroecosystems at 7 cropland eddy-covariance sites and 293
627 counties in the U.S. Midwest. Both the magnitude of simulated carbon flux/yield and their response

628 to the environmental variabilities had been compared with that from the observations. For site
629 scale simulation, the R^2 of the simulated GPP, NEE, Reco, and LAI is 0.92, 0.87, 0.87, and 0.78,
630 respectively. In addition, the dynamics of carbon allocation processes for both corn and soybean
631 can also be reproduced by *ecosys*. For the regional scale simulation, the spatial pattern and
632 interannual variance of crop yield are consistent with that from the USDA survey for both corn
633 and soybean. Specifically, the R^2 of the multi-year averaged simulated and observed yield is 0.83
634 and 0.80 for corn and soybean, respectively; while the R^2 of spatial-averaged simulated and
635 observed crop yield from 2001 to 2018 is 0.83 and 0.80 for corn and soybean, respectively. This
636 study is a strong demonstration of the ability of *ecosys* in simulating the carbon cycle for
637 agroecosystems. The response of carbon cycle processes/yield to the environmental variabilities
638 obtained from the simulations is consistent with that from the observations at both site-scale and
639 regional scale simulations, revealing the applicability of *ecosys* in simulating the impacts of future
640 climate change on the carbon cycle of the U.S. Midwestern agroecosystems. In addition, by
641 evaluating and constraining the majority carbon cycle process (i.e., GPP and yield at regional
642 scale), we are able to simulate the net biome productivity, which can be applied to quantify the
643 soil carbon sequestration of agroecosystems. The method and framework adopted in this study can
644 also be applied to other land surface models and terrestrial biosphere models to improve the
645 accounting of ecosystem carbon budget by integrating the mechanism models, observations, and
646 advanced machine learning tools.

647

648 **Acknowledgement:**

649 Authors acknowledge the support from the National Science Foundation (NSF) Career Award
650 (1847334), NASA Carbon Monitoring System Program (80NSSC18K0170), USDA National

651 Institute of Food and Agriculture (NIFA) Program (2017-67013-26253 and Hatch), Illinois
652 Nutrient Research & Education Council (NREC), and Department of Energy (DOE) (25-1215-
653 0208-006). Research reported in the publication was also partially supported by the Foundation
654 for Food and Agriculture Research under award number – Grant ID: 602757. The content of this
655 publication is solely the responsibility of the authors and does not necessarily represent the official
656 views of the Foundation for Food and Agriculture Research. We thank Andrew Suyker from
657 University of Nebraska Lincoln for providing the crop growth data at the Nebraska Mead flux-
658 tower sites, and Junrui Ni from University of Illinois for processing the USDA crop planting date
659 data at Illinois, Iowa, and Indiana. We acknowledge the following AmeriFlux sites for their data
660 records: US-Ne1, US-Ne1, US-Ne3, US-Bo1, US-Br1, US-Ib1, and US-Ro1. Funding for
661 AmeriFlux data resources was provided by the U.S. Department of Energy’s Office of Science.

662

663 **6. Reference**

664 Abdalla, M., Hastings, A., Cheng, K., Yue, Q., Chadwick, D., Espenberg, M., Truu, J., Rees, R.M.,
665 Smith, P., 2019. A critical review of the impacts of cover crops on nitrogen leaching, net
666 greenhouse gas balance and crop productivity. *Glob. Chang. Biol.* 25, 2530–2543.
667 <https://doi.org/10.1111/gcb.14644>

668 Allison, V.J., Michael Miller, R., Jastrow, J.D., Matamala, R., Zak, D.R., 2005. Changes in Soil
669 Microbial Community Structure in a Tallgrass Prairie Chronosequence. *Soil Science Society
670 of America Journal.* <https://doi.org/10.2136/sssaj2004.0252>

671 Anderson, J.P.E., Domsch, K.H., 1975. Measurement of bacterial and fungal contributions to
672 respiration of selected agricultural and forest soils. *Can. J. Microbiol.* 21, 314–322.
673 <https://doi.org/10.1139/m75-045>

674 Baker, J.M., Griffis, T.J., 2005. Examining strategies to improve the carbon balance of
675 corn/soybean agriculture using eddy covariance and mass balance techniques. *Agricultural*
676 *and Forest Meteorology*. <https://doi.org/10.1016/j.agrformet.2004.11.005>

677 Baker, J.M., Ochsner, T.E., Venterea, R.T., Griffis, T.J., 2007. Tillage and soil carbon
678 sequestration—What do we really know? *Agric. Ecosyst. Environ.* 118, 1–5.
679 <https://doi.org/10.1016/j.agee.2006.05.014>

680 Baldocchi, D.D., 2003. Assessing the eddy covariance technique for evaluating carbon dioxide
681 exchange rates of ecosystems: past, present and future. *Global Change Biology*.
682 <https://doi.org/10.1046/j.1365-2486.2003.00629.x>

683 Baldocchi, D., Falge, E., Gu, L., Olson, R., Hollinger, D., Running, S., Anthoni, P., Bernhofer, C.,
684 Davis, K., Evans, R., Fuentes, J., Goldstein, A., Katul, G., Law, B., Lee, X., Malhi, Y.,
685 Meyers, T., Munger, W., Oechel, W., Paw, K.T., Pilegaard, K., Schmid, H.P., Valentini, R.,
686 Verma, S., Vesala, T., Wilson, K., Wofsy, S., 2001. FLUXNET: A New Tool to Study the
687 Temporal and Spatial Variability of Ecosystem–Scale Carbon Dioxide, Water Vapor, and
688 Energy Flux Densities. *Bulletin of the American Meteorological Society*.
689 <https://doi.org/2.3.co;2>>10.1175/1520-0477(2001)082<2415:fanfts>2.3.co;2

690 Ball, J.T., 1988. *An Analysis of Stomatal Conductance*.

691 Bardgett, R.D., McAlister, E., 1999. The measurement of soil fungal:bacterial biomass ratios as
692 an indicator of ecosystem self-regulation in temperate meadow grasslands. *Biol. Fertil. Soils*
693 29, 282–290. <https://doi.org/10.1007/s003740050554>

694 Bernacchi, C.J., Hollinger, S.E., Meyers, T., 2005. The conversion of the corn/soybean ecosystem
695 to no-till agriculture may result in a carbon sink. *Global Change Biology*.
696 <https://doi.org/10.1111/j.1365-2486.2005.01050.x>

697 Blanco-Canqui, H., Lal, R., 2004. Mechanisms of Carbon Sequestration in Soil Aggregates.
698 Critical Reviews in Plant Sciences. <https://doi.org/10.1080/07352680490886842>

699 Brilli, L., Bechini, L., Bindi, M., Carozzi, M., Cavalli, D., Conant, R., Dorich, C.D., Doro, L.,
700 Ehrhardt, F., Farina, R., Ferrise, R., Fitton, N., Francaviglia, R., Grace, P., Iocola, I., Klumpp,
701 K., Léonard, J., Martin, R., Massad, R.S., Recous, S., Seddaiu, G., Sharp, J., Smith, P., Smith,
702 W.N., Soussana, J.-F., Bellocchi, G., 2017. Review and analysis of strengths and weaknesses
703 of agro-ecosystem models for simulating C and N fluxes. *Sci. Total Environ.* 598, 445–470.
704 <https://doi.org/10.1016/j.scitotenv.2017.03.208>

705 Chambers, A., Lal, R., Paustian, K., 2016. Soil carbon sequestration potential of US croplands and
706 grasslands: Implementing the 4 per ThoUSAnd Initiative. *J. Soil Water Conserv.* 71, 68A-
707 74A. <https://doi.org/10.2489/jswc.71.3.68A>

708 Deines, J.M., Wang, S., Lobell, D.B., 2019. Satellites reveal a small positive yield effect from
709 conservation tillage across the US Corn Belt. *Environ. Res. Lett.* 14, 124038.
710 <https://doi.org/10.1088/1748-9326/ab503b>

711 Dold, C., Büyükcangaz, H., Rondinelli, W., Prueger, J.H., Sauer, T.J., Hatfield, J.L., 2017. Long-
712 term carbon uptake of agro-ecosystems in the Midwest. *Agric. For. Meteorol.* 232, 128–140.
713 <https://doi.org/10.1016/j.agrformet.2016.07.012>

714 Drewniak, B., Song, J., Prell, J., Kotamarthi, V.R., Jacob, R., 2013. Modeling agriculture in the
715 Community Land Model. *Geosci. Model Dev.* 6, 495–515. [https://doi.org/10.5194/gmd-6-](https://doi.org/10.5194/gmd-6-495-2013)
716 [495-2013](https://doi.org/10.5194/gmd-6-495-2013)

717 Farquhar, G.D., von Caemmerer, S., Berry, J.A., 1980. A biochemical model of photosynthetic
718 CO₂ assimilation in leaves of C₃ species. *Planta*. <https://doi.org/10.1007/bf00386231>

719 Gilhespy, S.L., Anthony, S., Cardenas, L., Chadwick, D., del Prado, A., Li, C., Misselbrook, T.,

720 Rees, R.M., Salas, W., Sanz-Cobena, A., Smith, P., Tilston, E.L., Topp, C.F.E., Vetter, S.,
721 Yeluripati, J.B., 2014. First 20 years of DNDC (DeNitrification DeComposition): Model
722 evolution. *Ecol. Modell.* 292, 51–62. <https://doi.org/10.1016/j.ecolmodel.2014.09.004>

723 Grant, R.F., Lin, S., Hernandez-Ramirez, G., 2020. Modelling nitrification inhibitor effects on
724 N₂O emissions after fall-and spring-Applied slurry by reducing nitrifier NH₄⁺ oxidation rate.
725 *Biogeosciences* 17, 2021–2039. <https://doi.org/10.5194/bg-17-2021-2020>

726 Grant, R., 1997. Changes in Soil Organic Matter under Different Tillage and Rotation:
727 Mathematical Modeling in ecosys. *Soil Science Society of America Journal.*
728 <https://doi.org/10.2136/sssaj1997.03615995006100040023x>

729 Grant, R., Arkebauer, T., Dobermann, A., Hubbard, K., Schimelfenig, T., Suyker, A., Verma, S.,
730 Walters, D., 2007. Net Biome Productivity of Irrigated and Rainfed Maize-Soybean
731 Rotations: Modeling vs. Measurements. *Agronomy Journal.*
732 <https://doi.org/10.2134/agronj2006.0308>

733 Grant, R., Barr, A., Black, T., Margolis, H., McCaughey, J., Trofymow, J., 2010. Net ecosystem
734 productivity of temperate and boreal forests after clearcutting—a Fluxnet-Canada
735 measurement and modelling synthesis. *Tellus B.* <https://doi.org/10.3402/tellusb.v62i5.16588>

736 Grant, R.F., 2014. Nitrogen mineralization drives the response of forest productivity to soil
737 warming: Modelling in ecosys vs. measurements from the Harvard soil heating experiment.
738 *Ecol. Modell.* 288, 38–46. <https://doi.org/10.1016/j.ecolmodel.2014.05.015>

739 Grant, R.F., 2013. Modelling changes in nitrogen cycling to sustain increases in forest productivity
740 under elevated atmospheric CO₂ and contrasting site conditions. *Biogeosciences.*
741 <https://doi.org/10.5194/bg-10-7703-2013>

742 Grant, R.F., 2004. Modeling topographic effects on net ecosystem productivity of boreal black

743 spruce forests. *Tree Physiol.* 24, 1–18. <https://doi.org/10.1093/treephys/24.1.1>

744 Grant, R.F., 2001. A Review of the Canadian Ecosystem Model — ecosys. Modeling Carbon and
745 Nitrogen Dynamics for Soil Management. <https://doi.org/10.1201/9781420032635.ch6>

746 Grant, R.F., 1998. Simulation in ecosys of root growth response to contrasting soil water and
747 nitrogen. *Ecol. Modell.* 107, 237–264. [https://doi.org/10.1016/S0304-3800\(97\)00221-4](https://doi.org/10.1016/S0304-3800(97)00221-4)

748 Grant, R.F., 1995. Salinity, water use and yield of maize: Testing of the mathematical model
749 ecosys. *Plant and Soil.* <https://doi.org/10.1007/bf00011333>

750 Grant, R.F., 1989a. Test of a simple biochemical model for photosynthesis of maize and soybean
751 leaves. *Agric. For. Meteorol.* 48, 59–74. [https://doi.org/10.1016/0168-1923\(89\)90007-5](https://doi.org/10.1016/0168-1923(89)90007-5)

752 Grant, R.F., 1989b. Simulation of Carbon Assimilation and Partitioning in Maize. *Agronomy*
753 *Journal.* <https://doi.org/10.2134/agronj1989.00021962008100040004x>

754 Grant, R.F., 1989c. Simulation of Maize Phenology. *Agronomy Journal.*
755 <https://doi.org/10.2134/agronj1989.00021962008100030011x>

756 Grant, R.F., Baldocchi, D.D., Ma, S., 2012. Ecological controls on net ecosystem productivity of
757 a seasonally dry annual grassland under current and future climates: Modelling with ecosys.
758 *Agric. For. Meteorol.* 152, 189–200. <https://doi.org/10.1016/j.agrformet.2011.09.012>

759 Grant, R.F., Flanagan, L.B., 2007. Modeling stomatal and nonstomatal effects of water deficits on
760 CO₂ fixation in a semiarid grassland. *J. Geophys. Res. Biogeosciences* 112.
761 <https://doi.org/10.1029/2006JG000302>

762 Grant, R.F., Goulden, M.L., Wofsy, S.C., Berry, J.A., 2001. Carbon and energy exchange by a
763 black spruce-moss ecosystem under changing climate: Testing the mathematical model
764 ecosys with data from the BOREAS experiment. *J. Geophys. Res. Atmos.* 106, 33605–33621.
765 <https://doi.org/10.1029/2001JD900064>

766 Grant, R.F., Kimball, B.A., Conley, M.M., White, J.W., Wall, G.W., Ottman, M.J., 2011.
767 Controlled Warming Effects on Wheat Growth and Yield: Field Measurements and
768 Modeling. *Agronomy Journal*. <https://doi.org/10.2134/agronj2011.0158>

769 Grant, R.F., Neftel, A., Calanca, P., 2016. Ecological controls on N₂O emission in surface litter
770 and near-surface soil of a managed grassland: modelling and measurements. *Biogeosciences*
771 13, 3549–3571. <https://doi.org/10.5194/bg-13-3549-2016>

772 Grant, R.F., Pattey, E., 2008. Temperature sensitivity of N₂O emissions from fertilized
773 agricultural soils: Mathematical modeling in ecosys. *Global Biogeochem. Cycles* 22, n/a-n/a.
774 <https://doi.org/10.1029/2008GB003273>

775 Grant, R.F., Pattey, E., 2003. Modelling variability in N₂O emissions from fertilized agricultural
776 fields. *Soil Biol. Biochem.* 35, 225–243. [https://doi.org/10.1016/S0038-0717\(02\)00256-0](https://doi.org/10.1016/S0038-0717(02)00256-0)

777 Grant, R.F., Pattey, E., Goddard, T.W., Kryzanowski, L.M., Puurveen, H., 2006. Modeling the
778 Effects of Fertilizer Application Rate on Nitrous Oxide Emissions. *Soil Sci. Soc. Am. J.* 70,
779 235–248. <https://doi.org/10.2136/sssaj2005.0104>

780 Grant, R.F., Peters, D.B., Larson, E.M., Huck, M.G., 1989. Simulation of canopy photosynthesis
781 in maize and soybean. *Agric. For. Meteorol.* 48, 75–92. [https://doi.org/10.1016/0168-](https://doi.org/10.1016/0168-1923(89)90008-7)
782 [1923\(89\)90008-7](https://doi.org/10.1016/0168-1923(89)90008-7)

783 Grant, R.F., Rochette, P., 1994. Soil Microbial Respiration at Different Water Potentials and
784 Temperatures: Theory and Mathematical Modeling. *Soil Science Society of America Journal*.
785 <https://doi.org/10.2136/sssaj1994.03615995005800060015x>

786 Grant, R.F., Rochette, P., Desjardins, R.L., 1993. Energy Exchange and Water Use Efficiency of
787 Field Crops: Validation of a Simulation Model. *Agronomy Journal*.
788 <https://doi.org/10.2134/agronj1993.00021962008500040025x>

789 Grant, R.F., Goulden, M.L., Wofsy, S.C., Berry, J.A., 2001. Carbon and energy exchange by a
790 black spruce-moss ecosystem under changing climate: Testing the mathematical model
791 ecosys with data from the BOREAS experiment. *J. Geophys. Res. Atmos.* 106, 33605–33621.
792 <https://doi.org/10.1029/2001JD900064>

793 Grant, R., Juma, N.G., Robertson, J.A., Izaurrealde, R.C., McGill, W.B., 2001b. Long-Term
794 Changes in Soil Carbon under Different Fertilizer, Manure, and Rotation: Testing the
795 Mathematical Model ecosys with Data from the Breton Plots. *Soil Sci. Soc. Am. J.*, NATO
796 ASI Series Vol. I 38 65, 205–214. <https://doi.org/10.2136/sssaj2001.651205x>

797 Grant, R., Juma, N., Robertson, J., Izaurrealde, R., McGill, W., 2001c. Long-Term Changes in Soil
798 Carbon under Different Fertilizer, Manure, and Rotation. *Soil Science Society of America*
799 *Journal*. <https://doi.org/10.2136/sssaj2001.1872a>

800 Grant, R., Mekonnen, Z., Riley, W., 2019. Modeling Climate Change Impacts on an Arctic
801 Polygonal Tundra: 1. Rates of Permafrost Thaw Depend on Changes in Vegetation and
802 Drainage. *J. Geophys. Res. Biogeosci.* 124, 1308–1322.
803 <https://doi.org/10.1029/2018JG004644>

804 Grant, R.F., Wall, G.W., Kimball, B.A., Frumau, K.F.A., Pinter, P.J., Hunsaker, D.J., Lamorte,
805 R.L., 1999. Crop water relations under different CO₂ and irrigation: testing of ecosys with
806 the free air CO₂ enrichment (FACE) experiment. *Agric. For. Meteorol.* 95, 27–51.
807 [https://doi.org/10.1016/S0168-1923\(99\)00017-9](https://doi.org/10.1016/S0168-1923(99)00017-9)

808 Grant, R., Zhang, Y., Yuan, F., Wang, S., Hanson, P., Gaumont-Guay, D., Chen, J., Black, T.,
809 Barr, A., Baldocchi, D., Arain, A., 2006. Intercomparison of techniques to model water stress
810 effects on CO₂ and energy exchange in temperate and boreal deciduous forests. *Ecological*
811 *Modelling*. <https://doi.org/10.1016/j.ecolmodel.2006.02.035>

812 Griffis, T.J., Sargent, S.D., Baker, J.M., Lee, X., Tanner, B.D., Greene, J., Swiatek, E., Billmark,
813 K., 2008. Direct measurement of biosphere-atmosphere isotopic CO₂ exchange using the
814 eddy covariance technique. *Journal of Geophysical Research*.
815 <https://doi.org/10.1029/2007jd009297>

816 Gurung, R.B., Ogle, S.M., Breidt, F.J., Williams, S.A., Parton, W.J., 2020. Bayesian calibration
817 of the DayCent ecosystem model to simulate soil organic carbon dynamics and reduce model
818 uncertainty. *Geoderma* 376, 114529. <https://doi.org/10.1016/j.geoderma.2020.114529>

819 Hernandez-Ramirez, G., Hatfield, J.L., Parkin, T.B., Sauer, T.J., Prueger, J.H., 2011. Carbon
820 dioxide fluxes in corn–soybean rotation in the midwestern U.S.: Inter- and intra-annual
821 variations, and biophysical controls. *Agricultural and Forest Meteorology*.
822 <https://doi.org/10.1016/j.agrformet.2011.07.017>

823 Huang, Y., Yu, Y., Zhang, W., Sun, W., Liu, S., Jiang, J., Wu, J., Yu, W., Wang, Y., Yang, Z.,
824 2009. Agro-C: A biogeophysical model for simulating the carbon budget of agroecosystems.
825 *Agric. For. Meteorol.* 149, 106–129. <https://doi.org/10.1016/j.agrformet.2008.07.013>

826 Hutchinson, J.J., Campbell, C.A., Desjardins, R.L., 2007. Some perspectives on carbon
827 sequestration in agriculture. *Agric. For. Meteorol.* 142, 288–302.
828 <https://doi.org/10.1016/j.agrformet.2006.03.030>

829 Jandl, R., Rodeghiero, M., Martinez, C., Cotrufo, M.F., Bampa, F., van Wesemael, B., Harrison,
830 R.B., Guerrini, I.A., Richter, D.D., Jr, Rustad, L., Lorenz, K., Chabbi, A., Miglietta, F., 2014.
831 Current status, uncertainty and future needs in soil organic carbon monitoring. *Sci. Total*
832 *Environ.* 468-469, 376–383. <https://doi.org/10.1016/j.scitotenv.2013.08.026>

833 Jarecki, M.K., Lal, R., 2003. Crop Management for Soil Carbon Sequestration. *Critical Reviews*
834 *in Plant Sciences*. <https://doi.org/10.1080/713608318>

835

836 Jiang, C., Guan, K., Wu, G., Peng, B., Wang, S., 2021. A daily, 250 m and real-time gross primary
837 productivity product (2000–present) covering the contiguous United States. *Earth Syst. Sci.*
838 *Data* 13, 281–298. <https://doi.org/10.5194/essd-13-281-2021>

839 Jin, Z., Zhuang, Q., Wang, J., Archontoulis, S. V., Zobel, Z., Kotamarthi, V.R., 2017. The
840 combined and separate impacts of climate extremes on the current and future US rainfed
841 maize and soybean production under elevated CO₂. *Glob. Chang. Biol.* 23, 2687–2704.
842 <https://doi.org/10.1111/gcb.13617>

843 Kimble, J.M., Follett, R.F., Vernon Cole, C., 1998. *The Potential of U.S. Cropland to Sequester*
844 *Carbon and Mitigate the Greenhouse Effect*. CRC Press.

845 Kimm, H., Guan, K., Gentine, P., Wu, J., Bernacchi, C.J., Sulman, B.N., Griffis, T.J., Lin, C.,
846 2020. Redefining droughts for the U.S. Corn Belt: The dominant role of atmospheric vapor
847 pressure deficit over soil moisture in regulating stomatal behavior of Maize and Soybean.
848 *Agric. For. Meteorol.* 287, 107930. <https://doi.org/10.1016/j.agrformet.2020.107930>

849 Kuppel, S., Peylin, P., Chevallier, F., Bacour, C., Maignan, F., Richardson, A.D., 2012.
850 Constraining a global ecosystem model with multi-site eddy-covariance data.
851 <https://doi.org/10.5194/bg-9-3757-2012>

852 Lal, R., 2011. Sequestering carbon in soils of agro-ecosystems. *Food Policy*.
853 <https://doi.org/10.1016/j.foodpol.2010.12.001>

854 Lal, R., Follett, R.F., Stewart, B.A., Kimble, J.M., 2007. Soil carbon sequestration to mitigate
855 climate change and advance food security. *Soil Sci.* 172.

856 Lal, R., 2004. Soil carbon sequestration impacts on global climate change and food security.
857 *Science* 304, 1623–1627. <https://doi.org/10.1126/science.1097396>

858 Lal, R., 2002. Soil carbon dynamics in cropland and rangeland. *Environ. Pollut.* 116, 353–362.
859 [https://doi.org/10.1016/s0269-7491\(01\)00211-1](https://doi.org/10.1016/s0269-7491(01)00211-1)

860 Lal, R., 2001. World cropland soils as a source or sink for atmospheric carbon. *Advances in*
861 *Agronomy*. [https://doi.org/10.1016/s0065-2113\(01\)71014-0](https://doi.org/10.1016/s0065-2113(01)71014-0)

862 Li, C., Frohking, S., Crocker, G.J., Grace, P.R., Klír, J., Körchens, M., Poulton, P.R., 1997.
863 Simulating trends in soil organic carbon in long-term experiments using the DNDC model.
864 *Geoderma* 81, 45–60. [https://doi.org/10.1016/S0016-7061\(97\)00080-3](https://doi.org/10.1016/S0016-7061(97)00080-3)

865 Liu, X., Chen, F., Barlage, M., Zhou, G., Niyogi, D., 2016. Noah-MP-Crop: Introducing dynamic
866 crop growth in the Noah-MP land surface model. *J. Geophys. Res.* 121, 13,953-13,972.
867 <https://doi.org/10.1002/2016JD025597>

868 Liu, Y., Yu, Z., Chen, J., Zhang, F., Doluschitz, R., Axmacher, J.C., 2006. Changes of soil organic
869 carbon in an intensively cultivated agricultural region: a denitrification-decomposition
870 (DNDC) modelling approach. *Sci. Total Environ.* 372, 203–214.
871 <https://doi.org/10.1016/j.scitotenv.2006.09.022>

872 Li, Y., Guan, K., Schnitkey, G.D., DeLucia, E., Peng, B., 2019. Excessive rainfall leads to maize
873 yield loss of a comparable magnitude to extreme drought in the United States. *Glob. Chang.*
874 *Biol.* 25, 2325–2337. <https://doi.org/10.1111/gcb.14628>

875 Lobell, D.B., Roberts, M.J., Schlenker, W., Braun, N., Little, B.B., Rejesus, R.M., Hammer, G.L.,
876 2014. Greater sensitivity to drought accompanies maize yield increase in the U.S. Midwest.
877 *Science* 344, 516–519. <https://doi.org/10.1126/science.1251423>

878 Mäkelä, A., Pulkkinen, M., Kolari, P., Lagergren, F., Berbigier, P., Lindroth, A., Loustau, D.,
879 Nikinmaa, E., Vesala, T., Hari, P., 2007. Developing an empirical model of stand GPP with
880 the LUE approach: analysis of eddy covariance data at five contrasting conifer sites in Europe.

881 Glob. Chang. Biol. 0, 071124112207003-??? <https://doi.org/10.1111/j.1365->
882 2486.2007.01463.x

883 Meena, R.S., Kumar, S., Yadav, G.S., 2020. Soil Carbon Sequestration in Crop Production, in:
884 Meena, R.S. (Ed.), Nutrient Dynamics for Sustainable Crop Production. Springer Singapore,
885 Singapore, pp. 1–39. https://doi.org/10.1007/978-981-13-8660-2_1

886 Mehra, P., Baker, J., Sojka, R.E., Bolan, N., Desbiolles, J., Kirkham, M.B., Ross, C., Gupta, R.,
887 2018. A Review of Tillage Practices and Their Potential to Impact the Soil Carbon Dynamics,
888 in: Advances in Agronomy. Elsevier Inc., pp. 185–230.
889 <https://doi.org/10.1016/bs.agron.2018.03.002>

890 Mekonnen, Z.A., Grant, R.F., Schwalm, C., 2017. Carbon sources and sinks of North America as
891 affected by major drought events during the past 30 years. Agric. For. Meteorol. 244–245,
892 42–56. <https://doi.org/10.1016/j.agrformet.2017.05.006>

893 Meyers, T., 2004. An assessment of storage terms in the surface energy balance of maize and
894 soybean. Agricultural and Forest Meteorology.

895 Mezbahuddin, M., Grant, R.F., Flanagan, L.B., 2017. Coupled eco-hydrology and
896 biogeochemistry algorithms enable the simulation of water table depth effects on boreal
897 peatland net CO₂ exchange. Biogeosciences 14, 5507–5531. [https://doi.org/10.5194/bg-14-](https://doi.org/10.5194/bg-14-5507-2017)
898 5507-2017

899 Mezbahuddin, S., Spiess, D., Hildebrand, D., Kryzanowski, L., Itenfisu, D., Goddard, T., Iqbal, J.,
900 Grant, R., 2020. Assessing Effects of Agronomic Nitrogen Management on Crop Nitrogen
901 Use and Nitrogen Losses in the Western Canadian Prairies. Frontiers in Sustainable Food
902 Systems. <https://doi.org/10.3389/fsufs.2020.512292>

903 Osborne, B., Saunders, M., Walmsley, D., Jones, M., Smith, P., 2010. Key questions and

904 uncertainties associated with the assessment of the cropland greenhouse gas balance. *Agric.*
905 *Ecosyst. Environ.* 139, 293–301. <https://doi.org/10.1016/j.agee.2010.05.009>

906 Peng, B., Guan, K., Chen, M., Lawrence, D.M., Pokhrel, Y., Suyker, A., Arkebauer, T., Lu, Y.,
907 2018. Improving maize growth processes in the community land model: Implementation and
908 evaluation. *Agric. For. Meteorol.* 250-251, 64–89.
909 <https://doi.org/10.1016/j.agrformet.2017.11.012>

910 Peng, B., Guan, K., Tang, J., Ainsworth, E.A., Asseng, S., Bernacchi, C.J., Cooper, M., Delucia,
911 E.H., Elliott, J.W., Ewert, F., Grant, R.F., Gustafson, D.I., Hammer, G.L., Jin, Z., Jones, J.W.,
912 Kimm, H., Lawrence, D.M., Li, Y., Lombardozzi, D.L., Marshall-Colon, A., Messina, C.D.,
913 Ort, D.R., Schnable, J.C., Vallejos, C.E., Wu, A., Yin, X., Zhou, W., 2020. Towards a
914 multiscale crop modelling framework for climate change adaptation assessment. *Nat Plants*
915 6, 338–348. <https://doi.org/10.1038/s41477-020-0625-3>

916 Poeplau, C., Don, A., 2015. Carbon sequestration in agricultural soils via cultivation of cover crops
917 – A meta-analysis. *Agric. Ecosyst. Environ.* 200, 33–41.
918 <https://doi.org/10.1016/j.agee.2014.10.024>

919 Salmon, Y., Lintunen, A., Dayet, A., Chan, T., Dewar, R., Vesala, T., Hölttä, T., 2020. Leaf carbon
920 and water status control stomatal and nonstomatal limitations of photosynthesis in trees. *New*
921 *Phytol.* 226, 690–703. <https://doi.org/10.1111/nph.16436>

922 Seifert, C.A., Azzari, G., Lobell, D.B., 2019. Corrigendum: Satellite detection of cover crops and
923 their effects on crop yield in the Midwestern United States (2018 *Environ. Res. Lett.* 13
924 064033). *Environ. Res. Lett.* 14, 039501. <https://doi.org/10.1088/1748-9326/aaf933>

925 Schrumpf, M., Schulze, E.D., Kaiser, K., Schumacher, J., 2011. How accurately can soil organic
926 carbon stocks and stock changes be quantified by soil inventories? <https://doi.org/10.5194/bg->

927 8-1193-2011

928 Shekoofa, A., Safikhan, S., Snider, J.L., Raper, T.B., Bourland, F.M., 2021. Variation in stomatal
929 conductance responses of cotton cultivars to high vapour pressure deficit under controlled
930 and rainfed environments. *J. Agron. Crop Sci.* 207, 332–343.
931 <https://doi.org/10.1111/jac.12440>

932 Shirato, Y., 2005. Testing the Suitability of the DNDC Model for Simulating Long-Term Soil
933 Organic Carbon Dynamics in Japanese Paddy Soils. *Soil Sci. Plant Nutr.* 51, 183–192.
934 <https://doi.org/10.1111/j.1747-0765.2005.tb00022.x>

935 Stehfest, E., Heistermann, M., Priess, J.A., Ojima, D.S., Alcamo, J., 2007. Simulation of global
936 crop production with the ecosystem model DayCent. *Ecol. Modell.* 209, 203–219.
937 <https://doi.org/10.1016/j.ecolmodel.2007.06.028>

938 Suyker, A.E., Verma, S.B., 2012. Gross primary production and ecosystem respiration of irrigated
939 and rainfed maize–soybean cropping systems over 8 years. *Agricultural and Forest
940 Meteorology.* <https://doi.org/10.1016/j.agrformet.2012.05.021>

941 Suyker, A.E., Verma, S.B., Burba, G.G., Arkebauer, T.J., 2005. Gross primary production and
942 ecosystem respiration of irrigated maize and irrigated soybean during a growing season.
943 *Agricultural and Forest Meteorology.* <https://doi.org/10.1016/j.agrformet.2005.05.007>

944 Tarantola, A., 2013. *Inverse Problem Theory: Methods for Data Fitting and Model Parameter
945 Estimation.* Elsevier.

946 USDA, 2021. USDA National Agricultural Statistics Service National 2020 Cultivated Layer.
947 Available at https://www.nass.usda.gov/Research_and_Science/Cropland/Release/index.php
948 (accessed May 2021). USDA-NASS, Washington, DC.

949 USDA, 2020. Crop Production 2019 Summary.

950 https://www.nass.usda.gov/Publications/Todays_Reports/reports/cropan20.pdf

951 USDA, 2019. Fertilizer Use and Price. [https://www.ers.usda.gov/data-products/fertilizer-use-and-](https://www.ers.usda.gov/data-products/fertilizer-use-and-price/)

952 [price/](https://www.ers.usda.gov/data-products/fertilizer-use-and-price/)

953 VandenBygaart, A.J., Angers, D.A., 2006. Towards accurate measurements of soil organic carbon

954 stock change in agroecosystems. *Can. J. Soil Sci.* 86, 465–471. [https://doi.org/10.4141/S05-](https://doi.org/10.4141/S05-106)

955 106

956 van Wesemael, B., Paustian, K., Meersmans, J., Goidts, E., Barancikova, G., Easter, M., 2010.

957 Agricultural management explains historic changes in regional soil carbon stocks. *Proc. Natl.*

958 *Acad. Sci. U. S. A.* 107, 14926–14930. <https://doi.org/10.1073/pnas.1002592107>

959 Verma, S.B., Dobermann, A., Cassman, K.G., Walters, D.T., Knops, J.M., Arkebauer, T.J.,

960 Suyker, A.E., Burba, G.G., Amos, B., Yang, H., Ginting, D., Hubbard, K.G., Gitelson, A.A.,

961 Walter-Shea, E.A., 2005. Annual carbon dioxide exchange in irrigated and rainfed maize-

962 based agroecosystems. *Agric. For. Meteorol.* 131, 77–96.

963 <https://doi.org/10.1016/j.agrformet.2005.05.003>

964 Van den Hoof, C., Hanert, E., Vidale, P.L., 2011. Simulating dynamic crop growth with an adapted

965 land surface model – JULES-SUCROS: Model development and validation. *Agric. For.*

966 *Meteorol.* 151, 137–153. <https://doi.org/10.1016/j.agrformet.2010.09.011>

967 Vogel, F.A., 2018. Understanding USDA Crop Forecasts: March 1999 (Classic Reprint).

968 Forgotten Books.

969 Wang, S., Garcia, M., Ibrom, A., Bauer-Gottwein, P., 2020. Temporal interpolation of land surface

970 fluxes derived from remote sensing – results with an unmanned aerial system. *Hydrol. Earth*

971 *Syst. Sci.* 24, 3643–3661. <https://doi.org/10.5194/hess-24-3643-2020>

972 Wattenbach, M., Sus, O., Vuichard, N., Lehuger, S., Gottschalk, P., Li, L., Leip, A., Williams, M.,

973 Tomelleri, E., Kutsch, W.L., Buchmann, N., Eugster, W., Dietiker, D., Aubinet, M., Ceschia,
974 E., Béziat, P., Grünwald, T., Hastings, A., Osborne, B., Ciais, P., Cellier, P., Smith, P., 2010.
975 The carbon balance of European croplands: A cross-site comparison of simulation models.
976 *Agric. Ecosyst. Environ.* 139, 419–453. <https://doi.org/10.1016/j.agee.2010.08.004>

977 West, T.O., Bandaru, V., Brandt, C.C., Schuh, A.E., Ogle, S.M., 2011. Regional uptake and release
978 of crop carbon in the United States. *Biogeosciences*. <https://doi.org/10.5194/bg-8-2037-2011>

979 West, T.O., Brandt, C.C., Baskaran, L.M., Hellwinckel, C.M., Mueller, R., Bernacchi, C.J.,
980 Bandaru, V., Yang, B., Wilson, B.S., Marland, G., Nelson, R.G., De la Torre Ugarte, D.G.,
981 Post, W.M., 2010. Cropland carbon fluxes in the United States: increasing geospatial
982 resolution of inventory-based carbon accounting. *Ecol. Appl.* 20, 1074–1086.
983 <https://doi.org/10.1890/08-2352.1>

984 West, T.O., Brandt, C.C., Wilson, B.S., Hellwinckel, C.M., Tyler, D.D., Marland, G., De La Torre
985 Ugarte, D.G., Larson, J.A., Nelson, R.G., 2008. Estimating Regional Changes in Soil Carbon
986 with High Spatial Resolution. *Soil Sci. Soc. Am. J.* 72, 285–294.
987 <https://doi.org/10.2136/sssaj2007.0113>

988 West, T.O., Brown, M.E., Duren, R.M., Ogle, S.M., Moss, R.H., 2013. Definition, capabilities and
989 components of a terrestrial carbon monitoring system. *Carbon Management*.
990 <https://doi.org/10.4155/cmt.13.36>

991 West, T.O., Marland, G., 2002. A synthesis of carbon sequestration, carbon emissions, and net
992 carbon flux in agriculture: comparing tillage practices in the United States. *Agric. Ecosyst.*
993 *Environ.* 91, 217–232. [https://doi.org/10.1016/S0167-8809\(01\)00233-X](https://doi.org/10.1016/S0167-8809(01)00233-X)

994 Xue, F., Tong, L., Liu, W., Cao, H., Song, L., Ji, S., Ding, R., 2021. Stomatal conductance of
995 tomato leaves is regulated by both abscisic acid and leaf water potential under combined

996 water and salt stress 1–9. <https://doi.org/10.1111/ppl.13441>

997 Yokohata, T., Kinoshita, T., Sakurai, G., Pokhrel, Y., Ito, A., Okada, M., Satoh, Y., Kato, E., Nitta,
998 T., Fujimori, S., Felfelani, F., Masaki, Y., Iizumi, T., Nishimori, M., Hanasaki, N., Takahashi,
999 K., Yamagata, Y., Emori, S., 2020. MIROC-INTEG-LAND version 1: a global
1000 biogeochemical land surface model with human water management, crop growth, and land-
1001 use change. *Geosci. Model Dev.* 13, 4713–4747. <https://doi.org/10.5194/gmd-13-4713-2020>

1002 Zhang, X., Izaurrealde, R.C., Manowitz, D.H., Sahajpal, R., West, T.O., Thomson, A.M., Xu, M.,
1003 Zhao, K., LeDuc, S.D., Williams, J.R., 2015. Regional scale cropland carbon budgets:
1004 Evaluating a geospatial agricultural modeling system using inventory data. *Environmental*
1005 *Modelling & Software* 63, 199–216. <https://doi.org/10.1016/j.envsoft.2014.10.005>

1006 Zhang, Y., Gurung, R., Marx, E., Williams, S., Ogle, S.M., Paustian, K., 2020. DayCent Model
1007 Predictions of NPP and Grain Yields for Agricultural Lands in the Contiguous U.S. *J.*
1008 *Geophys. Res. Biogeosci.* <https://doi.org/10.1029/2020JG005750>

1009 Zhou, W., Guan, K., Peng, B., Shi, J., Jiang, C., Wardlow, B., Pan, M., Kimball, J.S., Franz, T.E.,
1010 Gentine, P., He, M., Zhang, J., 2020. Connections between the hydrological cycle and crop
1011 yield in the rainfed U.S. Corn Belt. *J. Hydrol.* 590, 125398.
1012 <https://doi.org/10.1016/j.jhydrol.2020.125398>